PHILOSOPHICAL TRANSACTIONS OF THE ROYAL SOCIETY A MATHEMATICAL, PHYSICAL & ENGINEERING SCIENCES

On the Flow of Molten Polymer into, within and out of Ducts

N. Checker, M. R. Mackley and D. W. Mead

Phil. Trans. R. Soc. Lond. A 1983 **308**, 451-477
doi: 10.1098/rsta.1983.0015

Phil. Trans. R. Soc. Lond. A **308**, 451–477 (1983) [451]
Printed in Great Britain

ON THE FLOW OF MOLTEN POLYMER INTO, WITHIN AND OUT OF DUCTS

BY N. CHECKER†, M. R. MACKLEY‡ AND D. W. MEAD‡

† *School of Engineering and Applied Sciences, University of Sussex, Brighton, Sussex BN1 9RH, U.K.*

‡ *Department of Chemical Engineering, University of Cambridge, Pembroke Street, Cambridge CB3 2RA, U.K.*

Communicated by J. F. Davidson, F.R.S. – Received 25 January 1982)

[Plates 1–8]

CONTENTS

We report experimental observations on the flow of molten polyethylene and polypropylene into, within and out of two-dimensional ducts. Using flow birefringence techniques we follow as a function of flow rate, temperature and molecular weight§ the evolution and relaxation of molecular orientation as the polymer flows through and out of the duct. In particular we are interested in the flow along the centre line of the duct where within the duct we are able to determine readily relaxation times for the polymer melt. Our observations show that the 'short-time-scale' relaxation behaviour of the melt depends on the magnitude of the entrance velocity gradient but is essentially independent of both temperature and the 'molecular weight' averages of the polymer. The 'long-time-scale' relaxation behaviour is found

§ Correctly relative molecular mass.

to have a different dependence. To explain our relaxation time and die swell results we propose that the molten polymer forms a composite material that in the quiescent state consists of a molecular network embedded in a matrix of polymer chains of lower molecular weight. The network and matrix respond to the imposed velocity history in different ways.

1. Introduction

Our primary objective is to understand how molten polymers respond to different velocity fields. To gain some insight into the problem we chose a flow geometry that in our opinion has sufficient simplicity to enable detailed analysis while containing a range of velocity fields that are of interest to us and that would also be experienced in most commercial processing devices. Our main experimental technique is that of flow birefringence and this dictates that, to make optical interpretation of our observations straightforward, the flow should be essentially two-dimensional. We chose to examine the flow of polymer within the geometry shown schematically in figure 1. Molten polymer enters the duct at an essentially uniform and low

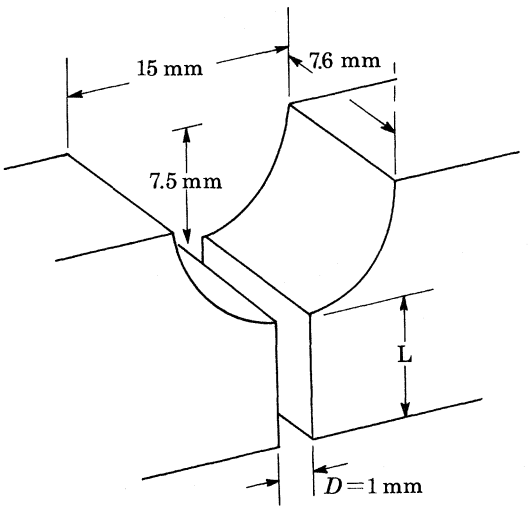

Figure 1. Schematic diagram of duct showing entrance and slit dimensions.

velocity. The polymer then experiences a changing cross-sectional area in the duct and consequently a dominantly extensional velocity field is established upstream of the throat. The semicircular duct entrance profile is chosen as a compromise between wanting the bounding surface to be distant from the entrance region but not wanting a stagnant zone or recirculation to develop at certain flow rates, which would be the case if a square duct entrance profile was chosen (see for example Tordella 1957; Clegg 1958). Downstream of the throat and within the slit the velocity field quickly changes to that of steady simple shearing flow near the walls and zero velocity gradient along the centre line of the slit section. This latter aspect is of particular interest to us, as by following the behaviour of the melt along the centre line of the duct we are able to follow the 'free relaxation' of the polymer that had been oriented in the entrance region. The velocity field at the exit of the duct where the polymer emerges into free space is complex and will be discussed later.

The geometry chosen is central to many viscometric measuring devices as well as commercial processes. Consequently it is not surprising that it has received extensive attention in the

literature. In the context of the work to be described the observations of Han & Drexler (1973) and Brizitsky *et al.* (1978) are relevant. Both groups of workers used flow birefringence techniques to examine stress patterns in two-dimensional ducts; our work extends their findings and also examines the results from a different view-point. The related rheological work associated with pressure-drop measurements along dies and ducts is extensive and Han (1976) represents one review of the subject. Similarly the flow of molten polymer out of a duct and its subsequent die swell into free space has exercised the minds of rheologists for several decades. The reviews of Boger & Denn (1980) and Middleman (1977) are representative appraisals of the subject.

It is not the primary purpose of this paper to propose a rheological model of the polymer melt; however, it is certainly true that any chosen rheological model will be required to explain the time-dependent behaviour that we observe. In terms of steady-state properties, which again is not our primary concern here, two important quantities will also have to be described; namely the steady-state simple shearing viscosity of the polymer which can be mathematically described adequately by the empirical Cross (1970) equation,

$$\eta = \eta_\infty + (\eta_0 - \eta_\infty)/(1 + \alpha\dot{\epsilon}^m), \tag{1}$$

where η is the apparent viscosity at a simple shearing rate $\dot{\epsilon}$, η_0 and η_∞ are limiting viscosities at zero and infinite shear rates respectively, and α and m are constants.

Secondly, and of greater direct relevance to the work of this paper, in steady simple shearing flow the polymer melt must satisfy the so called stress optical law given by

$$\eta_{ii} - \eta_{jj} = C(\sigma_{ii} - \sigma_{jj}), \tag{2}$$

where $\eta_{ii} - \eta_{jj}$ is the principal refractive-index difference of the melt, $\sigma_{ii} - \sigma_{jj}$ is the corresponding principal stress difference and C is the stress optical coefficient, which has been found by Wales (1976) to depend on the particular polymer chosen. Wales has also found that C is independent of molecular weight distribution but can change with temperature.

The main variables that effect the flow of molten polymer through ducts are listed below:

polymer	chemical species, molecular weight distribution
duct geometry	entrance region
	L/D of slit
	exit region
external	volumetric flow rate
	temperature
	absolute pressure
other factors	previous thermal and shear history
	downstream conditions outside duct.

We have made a systematic study of various grades of polymer flowing in a specified geometry of duct having different length/diameter (L/D) ratios. In addition we have examined the effect of volumetric flow rate and temperature. We have not yet examined in detail the effect of absolute pressure or previous thermal and shear history, the latter in our opinion being of great importance. In this paper we also limit ourselves to an entrance region where the change in cross-sectional area is fixed at a factor of 15. From our findings we also believe that this change is a very important variable and deserves further close examination.

PHILOSOPHICAL TRANSACTIONS OF THE ROYAL SOCIETY A MATHEMATICAL, PHYSICAL & ENGINEERING SCIENCES

2. Experimental

A schematic diagram of the block containing the duct is shown in figure 2. Polymer is fed to the block from a Davenport rheometer, which is capable of supplying the melt under isothermal conditions and at a controlled flow rate. After passing through a short connecting tube, of circular section, the polymer enters the block and then flows into a spark-eroded hole where the circular section of diameter 18 mm changes to a rectangular section of width 15 mm and

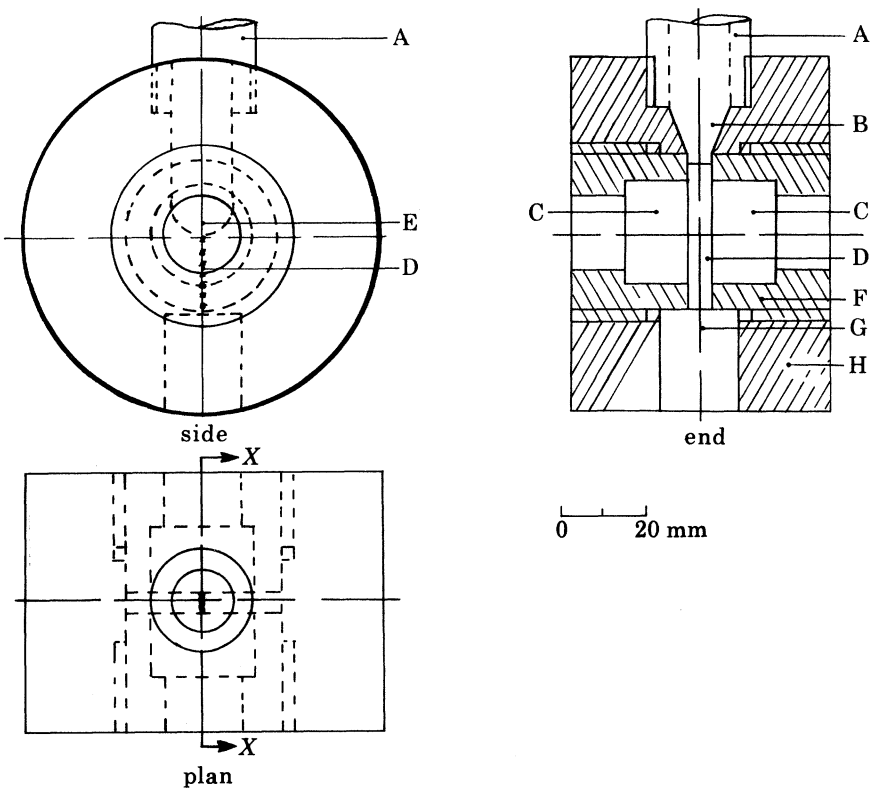

Figure 2. Schematic diagram of block containing duct. A, rheometer attachment; B, spark eroded hole; C, window, D, slit; E, slit entry, F, window holder, G, slit exit, H, main block. End elevation section taken at *XX*.

depth 7.6 mm over a distance of 10 mm. The area under optical examination is bounded on both front and back faces by circular glass windows that are 15 mm thick, and the metal profile of the chosen duct is sandwiched between the windows' flat faces. The slit section has width 1 mm and depth 7.6 mm, the latter being dictated by the need for a suitable thickness of melt to give a convenient number of retardation bands when the melt was viewed between crossed polaroids during flow. We encountered experimental difficulties in observing exit effects and the experimental arrangements for these observations will be described in the appropriate section. A band heater was attached to the outer circumference of the block and temperature control of the whole system was considered to be better than ± 1 K over the range 20–300 °C.

3. Observations

3.1. *Velocity profiles within duct*

We wish to relate our flow birefringence measurements to the velocity gradient and strain history of the melt. To do this knowledge of the velocity field within the duct is necessary. In this study we report findings based on particle-track measurements. The technique has serious limitations in that it is suitable in our system only up to velocities of the order 10 mm/s, well below most velocities used in the birefringence studies. We include the measurements to give an overall impression of the form of the velocity profiles present. More detailed investigation with laser velocimetry equipment is currently being undertaken.

The optical arrangement is shown schematically in figure 3*a* for the particle-track photography and figure 3*b* for the flow birefringence measurements. For the velocity measurements the duct was illuminated by passing a collimated laser beam vertically upwards through the

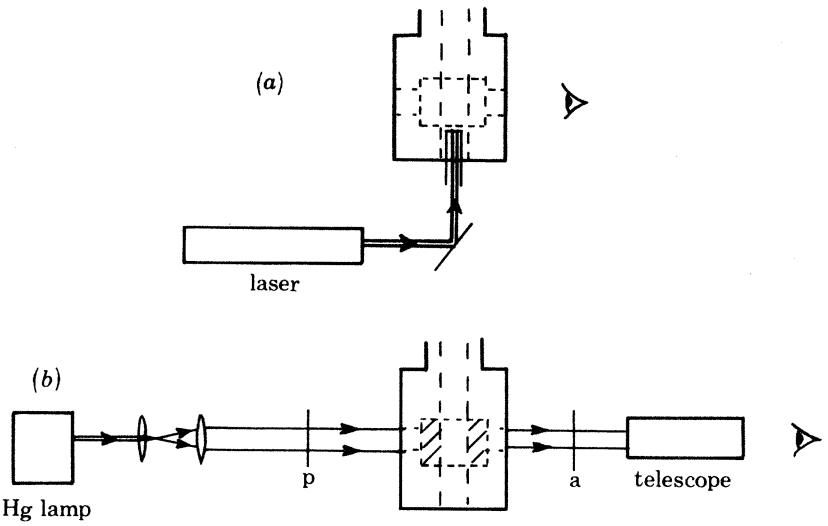

Figure 3. Optical arrangement for (*a*) particle track photography and (*b*) flow birefringence measurements. p, Polarizer; a, analyser.

exit of the duct. A small amount of copper-powder particles was introduced into the melt and by suitable choice of camera exposure time observed particle track lengths could easily be converted into velocities.

Figure 4 shows the measured velocity profile along the centre line of the duct for several different volumetric flow rates through the duct. The material used was high density polyethylene (HDPE) Rigidex 006. $\bar{M}_w = 130000$, $\bar{M}_n = 20000$, at a temperature of 170 °C. Zero distance on the figure corresponds to the position of the throat. Figure 5 shows the corresponding axial longitudinal velocity gradient.

The centre-line profile shows several relevant features. Within the entrance region the velocity increases non-uniformly, leading to a longitudinal velocity gradient that increases, reaches a maximum and then rapidly decreases to zero within the slit where the velocity along the centre line is uniform. To characterize the velocity gradients in the entrance region, at any given flow rate the maximum velocity gradient $\dot{\epsilon}_m$ is taken as a representative magnitude for the overall velocity gradient field in the entrance. This is equivalent to saying that the velocity

gradient starts at zero, reaches $\dot{\epsilon}_m$ instantly, maintains this value until the throat is reached and then instantly decreases to zero. At this preliminary stage we feel this assumption is sufficient for the level of precision claimed in the subsequent analysis of our results. It can also be seen from the results shown in figure 5 that $\dot{\epsilon}_m$ varies linearly with the mean velocity $\bar{V}$. We make the further assumption that this relation can be extrapolated to higher velocities than those that we were able to measure experimentally.

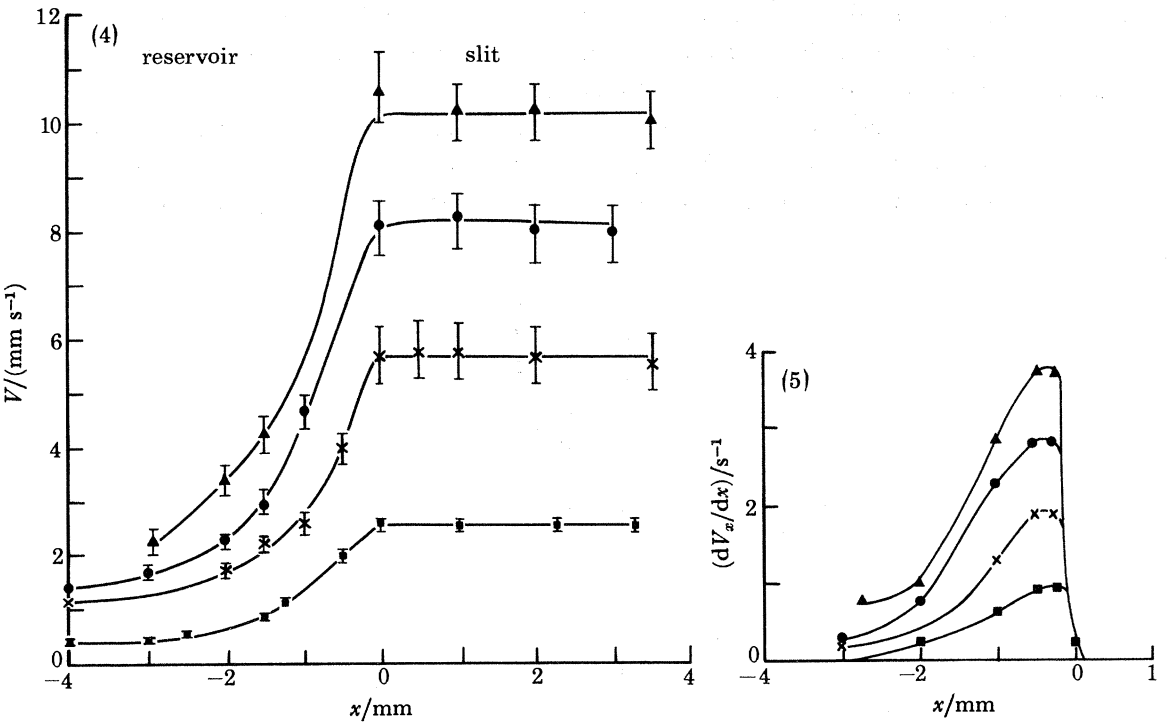

FIGURE 4. Axial centre line velocity profile, V, within duct for HDPE 006 ($\bar{M}_w = 13 \times 10^4$, $\bar{M}_n = 2 \times 10^4$) at 170 °C for four different volumetric flow rates $v/(\text{mm}^3/\text{s})$, ■, 13.6; ×, 27.2; ●, 44.8; ▲, 54.4. Throat of duct is at $x = 0$, x increasing in the downstream direction. Bars indicate vertical error.

FIGURE 5. Axial centre line velocity gradient, $\partial V_x/\partial x$, for the conditions of figure 4. Symbols are explained in figure 4.

At the throat of the duct interesting and initially unexpected transverse velocity profiles were discovered (see later section on instabilities); however, the transverse velocity profile within the slit will usually have reached an essentially steady semi-parabolic form after about 5 mm from the entrance. Figure 6 shows a series of measured transverse velocity profiles for different volumetric flows at a position 5 mm downstream of the throat. Figure 7 shows the corresponding magnitude of the simple shearing velocity gradient $\dot{\gamma} = \partial V_x/\partial y$. As would be expected the simple shearing velocity gradient is a maximum at the walls and progressively decreases to zero at the centre line of the slit. In addition, from these results it is evident that for a given flow rate the magnitude of the extensional velocity gradient $\dot{\epsilon}_m$ is about one fifth that of the simple shearing velocity gradient at the walls.

3.2. *Flow birefringence in the entrance region*

When a flowing melt is observed between crossed polaroids there is one of two reasons why total darkness can be observed. Firstly, if in a localized region a principal optic axis of the

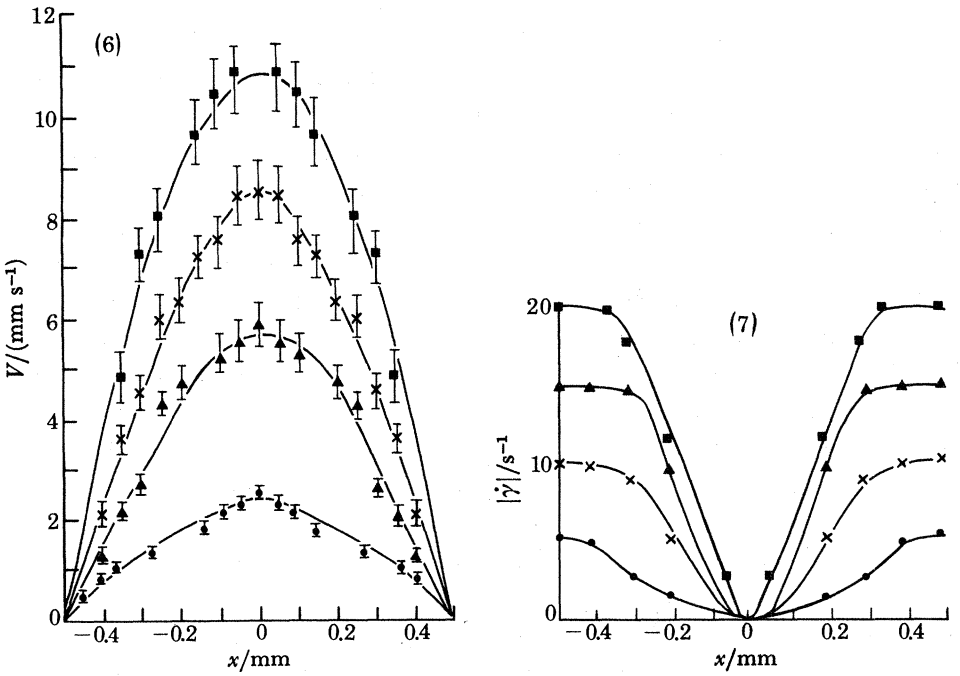

FIGURE 6. Transverse velocity profile within slit 5 mm down from throat for the conditions of figure 4 and volumetric flow rates $\bar{v}/(\mathrm{mm}^3/\mathrm{s})$, ●, 13.6; ▲, 27.2; ×, 44.8; ■, 54.4.

FIGURE 7. Modulus of transverse velocity gradient, γ, across slit for the conditions of figure 4 and volumetric flow rates $\bar{v}/(\mathrm{mm}^3/\mathrm{s})$, ●, 13.6; ×, 27.2; ▲, 44.8; ■, 54.4.

melt is parallel or perpendicular to the polarizer, darkness will be seen in that area; we term these regions of darkness extinction bands. Alternatively, if the principal optic axis of the melt does not coincide with the direction of either of the polaroids, dark regions will be seen where the optical retardation of the melt is an integral number N of wavelengths λ of the incident light, i.e.

$$\int_0^d \Delta(x)\,\mathrm{d}x = N\lambda, \quad N = 0, 1, 2 \ldots, \tag{3}$$

or $\Delta d = N\lambda$ if Δ is independent of x, where Δ is the birefringence and d is the depth of melt examined (in our case 7.6 mm). We term these dark regions retardation bands to distinguish them from extinction bands. It is straightforward to identify the two types of bands as extinction bands follow directly the movement of the polaroids when they are rotated, whereas the retardation bands have a much weaker dependence. Alternatively, by viewing the system between crossed circular polaroids the extinction bands are eliminated. In our optical analysis we also assume that the flow and hence optical anisotropy are two-dimensional. This of course is not true owing to the shearing at the two glass walls. However, Wales (1976) has shown that the corrections necessary for the effect can be expected to be small.

As in photoelasticity a retardation band corresponds to a region where the optical anisotropy is constant and, from the stress optical law, where the principal stress difference is constant. As the band number N increases from zero, the corresponding stress levels increase. By gradually increasing or decreasing the flow from the static or steady state it is possible to determine the value of N for any flow. It is sometimes useful to establish if a series of bands corresponds to an increasing or decreasing retardation. This can be established by using white

rather than monochromatic light. The bands then rather than being monochromatic are coloured and the direction of increasing retardation corresponds to the direction moving from the red side of the band to the blue side. We can interpret increasing optical anisotropy of the melt either in terms of increasing stresses given by the stress optical law or in terms of increasing levels of molecular orientation for the polymer chains within the melt. We defer detailed discussion of this aspect until after the experimental results are presented.

Within the entrance region the overall form of the optical retardation distribution as a function of flow rate, temperature and molecular weight is shown in figures 8, 9 and 10 respectively (plates 1 and 2). In all of the photographs the polaroids are oriented at 45° to the axis of the duct. The dominant direction of orientation of the molecules within the entrance region of the duct is along the stream lines of the flow and consequently the only extinction bands visible occur upstream of the throat emanating at about 45° from each of the edges of the throat. In the upstream region a series of retardation loops with ends at each throat edge are clearly visible; the retardation band number progressively increases as the throat is approached, indicating that the stresses and orientation are highest at the throat.

In figure 8, as anticipated, the stress and orientation levels increase with increasing flow rate. Figure 8*c* is of particular interest as it shows that at the edge of the throat a very severe stress gradient must exist because both the first and twenty-first fringes exist within less than, say, 0.1 mm of each other. In figure 9 the effect of temperature is apparent. With decreasing temperature the stress level increases and when the crystallization temperature is approached the onset of fibrous crystallization is observed as shown in figure 9*c*. The details of the mechanisms associated with the formation of fibrous crystals from the melt have been examined elsewhere (Mackley *et al.* 1975).

The effect of molecular weight shown in figure 10 is striking and of relevance. Increasing molecular weight leads to higher stresses as anticipated. However figure 10*c* shows clearly that for the high molecular weight material, even at $T = 170$ °C, which is some 35 °C above the melting range of HDPE, the melt can no longer be considered to be uniform. The retardation bands are no longer smooth and there are local 'spikes' in the bands. These spikes appear the follow streamlines of the flow and they correspond to regions along the streamline where the molecular orientation is greater than in the local surroundings. In view of the high temperature we do not necessarily identify these regions with fibrous crystallization. These areas represent inhomogeneities in the flow where the local orientation along certain streamlines is enhanced.

Our main interest is to follow in detail the behaviour of molten polymer that passes along the central streamline of the duct. It is therefore appropriate to plot the axial birefringence as a function of the variables examined. Figure 11 shows the variation of birefringence along the centre line for four volumetric flow rates. The birefringence builds up to a maximum at the throat and subsequently relaxes downstream of the throat. From figures 11 and 4 it can immediately be seen that there is a close comparison between the birefringence levels in the

Description of plate 1

Figure 8. Flow birefringence within duct: effect of mean flow (HDPE 006, $T = 170$ °C). (*a*) $\bar{v} = 10.1$ mm³/s, (*b*) $\bar{v} = 101$ mm³/s, (*c*) $\bar{v} = 395$ mm³/s. Polars are crossed at 45° to centre line.

Figure 9. Flow birefringence within duct: effect of temperature (HDPE 006, $\bar{v} = 395$ mm³/s). (*a*) $T = 190$ °C, (*b*) $T = 150$ °C, (*c*) $T = 140$ °C. Polars are crossed at 45° to centre line.

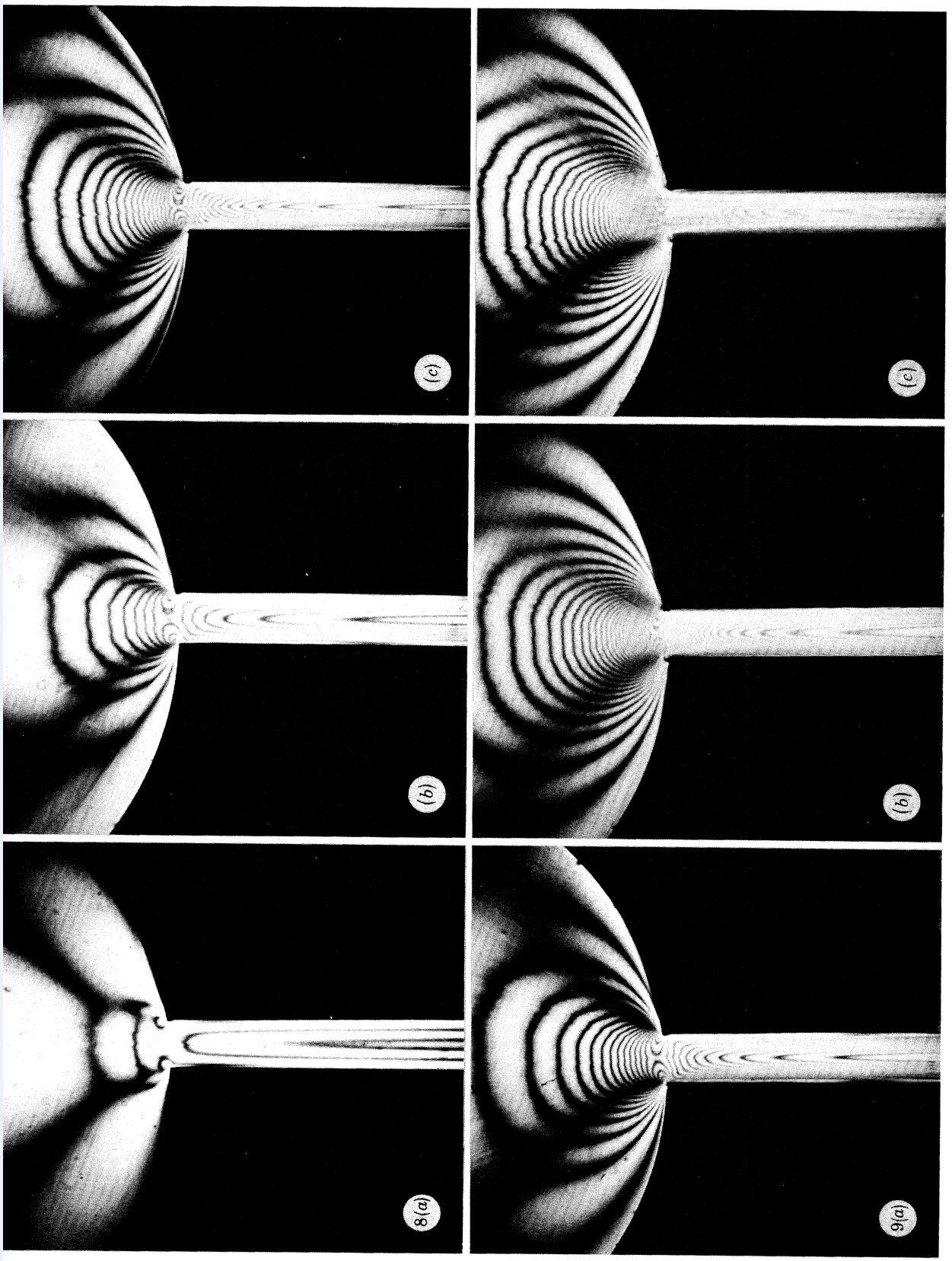

FIGURES 8 and 9. For description see opposite.

(*Facing p.* 458)

PHILOSOPHICAL TRANSACTIONS OF THE ROYAL SOCIETY A MATHEMATICAL, PHYSICAL & ENGINEERING SCIENCES

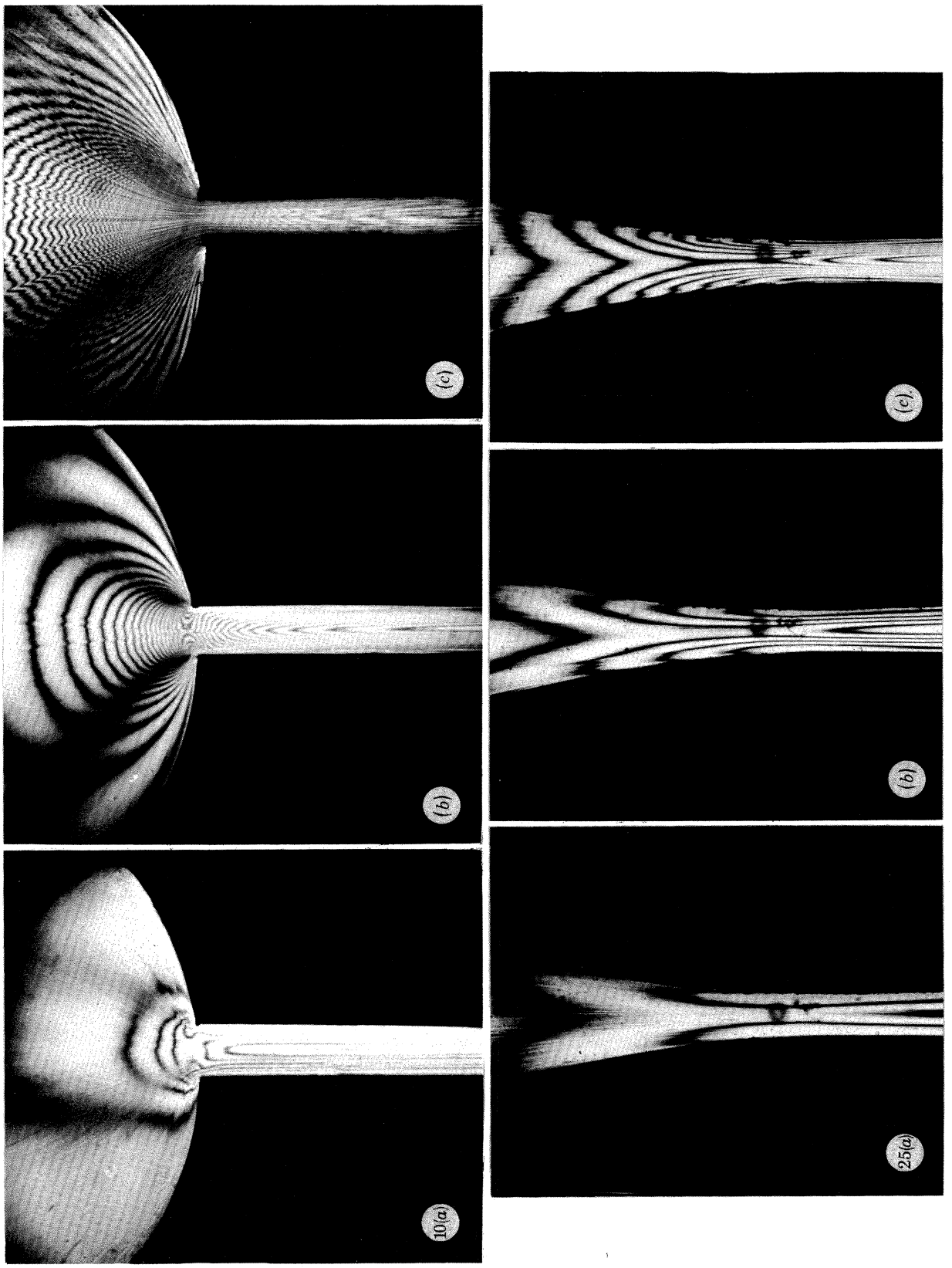

FIGURES 10 and 25. For description see opposite.

PHILOSOPHICAL TRANSACTIONS OF THE ROYAL SOCIETY A MATHEMATICAL, PHYSICAL & ENGINEERING SCIENCES

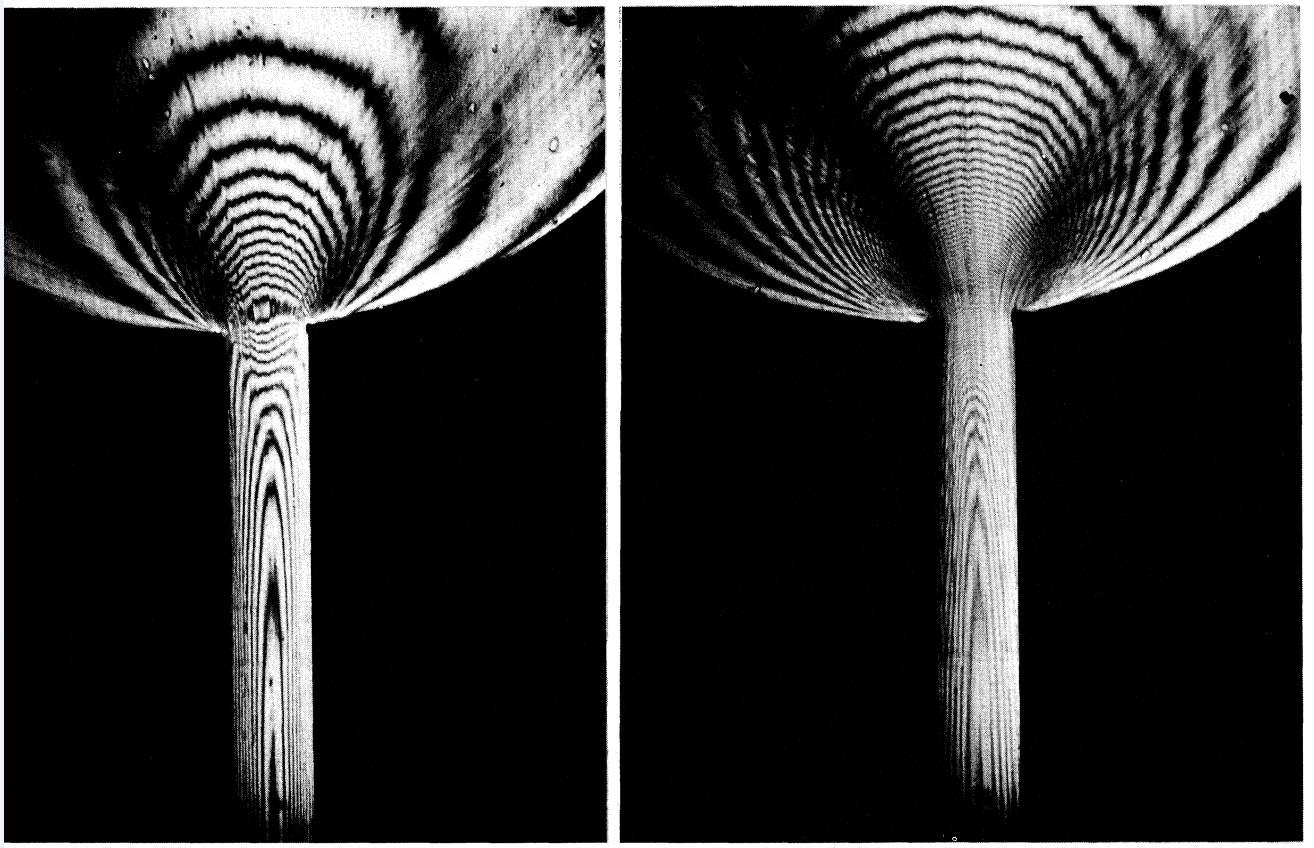

FIGURE 26. Flow birefringence showing 'symmetric oscillation' effect for HDPE 20–54P at 190 °C with $\bar{v} = 258$ mm³/s. Polars are crossed at 45°.

PHILOSOPHICAL TRANSACTIONS OF THE ROYAL SOCIETY A MATHEMATICAL, PHYSICAL & ENGINEERING SCIENCES

DESCRIPTION OF PLATE 2

FIGURE 10. Flow birefringence within duct: effect of relative molecular mass ($\bar{v} = 395$ mm³/s, $T = 170$ °C). (*a*) HDPE 140–60 ($\bar{M}_n = 1.4 \times 10^4$, $\bar{M}_w = 6.5 \times 10^4$), (*b*) HDPE 006 ($\bar{M}_n = 2 \times 10^4$, $\bar{M}_w = 13 \times 10^4$), (*c*) HDPE 20–54P ($\bar{M}_n = 3.2 \times 10^4$, $\bar{M}_w = 29 \times 10^4$). Polars are crossed at 45° to centre line.

FIGURE 25. Flow birefringence observed for tapered entrance for HDPE 006 at 190 °C: (*a*) $\bar{v} = 42.6$ mm³/s, (*b*) 130 mm³/s, (*c*) 517 mm³/s. Polars are crossed at 45°.

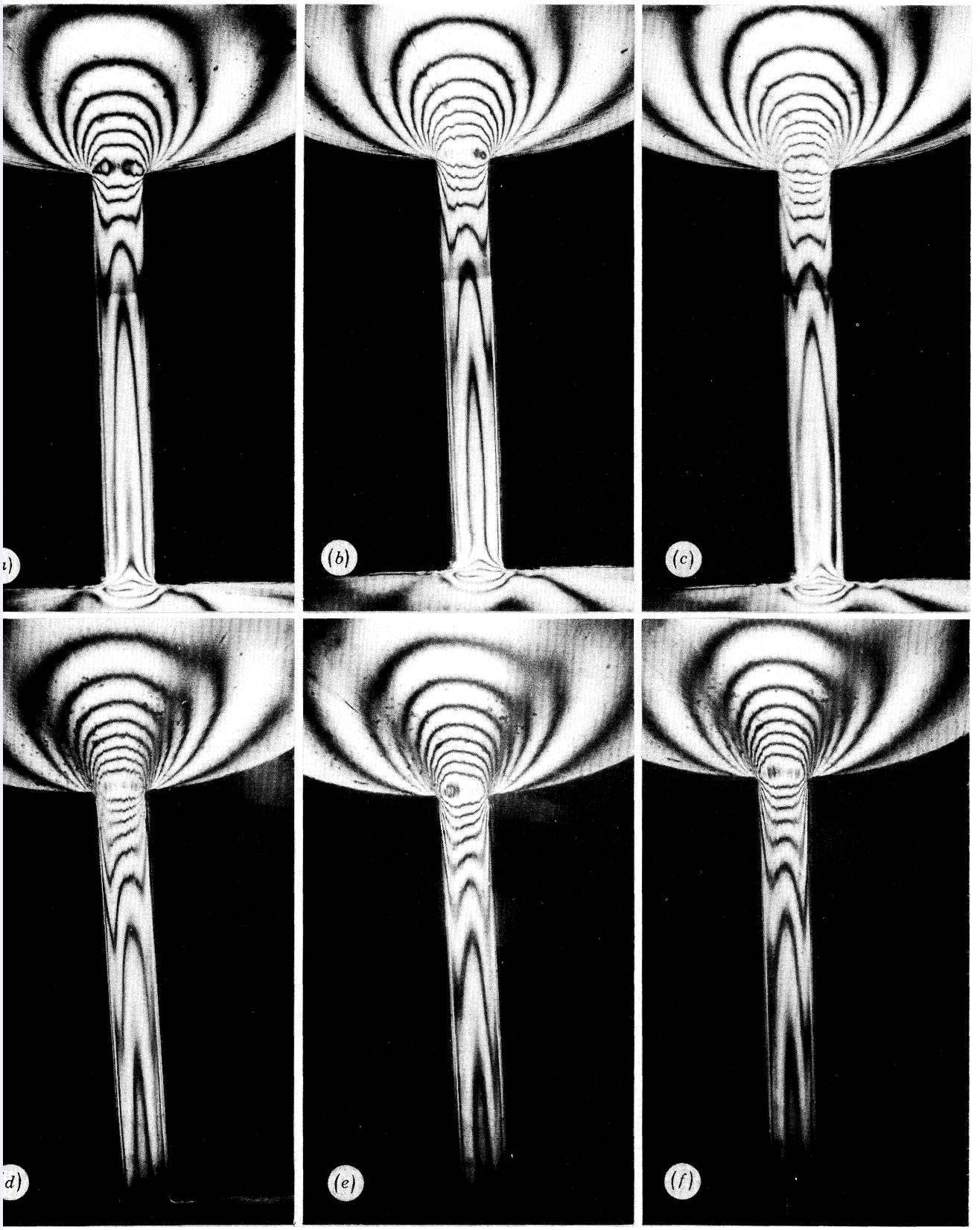

FIGURE 27. Development of W fringes and 'asymmetrical oscillations' for polypropylene copolymer GPE-102 at 193 °C: (*a*) $\bar{v} = 300$ mm³/s, (*b*) $\bar{v} = 400$ mm³/s, (*c*) $\bar{v} = 500$ mm³/s. (*d*)–(*f*) $\bar{v} = 510$ mm³/s, Polars are crossed at 4°5.

PHILOSOPHICAL TRANSACTIONS OF THE ROYAL SOCIETY A MATHEMATICAL, PHYSICAL & ENGINEERING SCIENCES

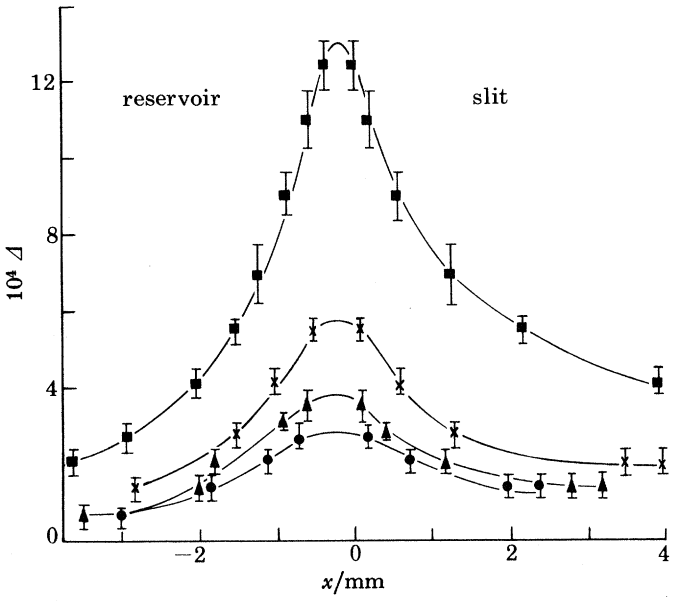

FIGURE 11. Birefringence, Δ, as a function of position along centre line of duct for HDPE 006 at 170 °C for volumetric flow rates $\bar{v}/(\mathrm{mm}^3/\mathrm{s})$, ●, 40.8; ▲, 54.4; ×, 136; ■, 576.

entrance region and the velocity gradients present. We chose to characterize the overall level of birefringence achieved in the entrance region by the value of the maximum birefringence Δ_m measured at the throat. This is plotted in figures 12 and 13 as a function of entrance velocity gradient $\dot{\epsilon}_m$ for different volumetric flow rates and for two different molecular weight distributions of HDPE.

The most important feature contained in these data is that Δ_m increases with increasing $\dot{\epsilon}_m$. However, at high values of $\dot{\epsilon}_m$ there are indications that the birefringence, and hence orientation, are approaching maximum values and becoming independent of $\dot{\epsilon}_m$. In addition, for a

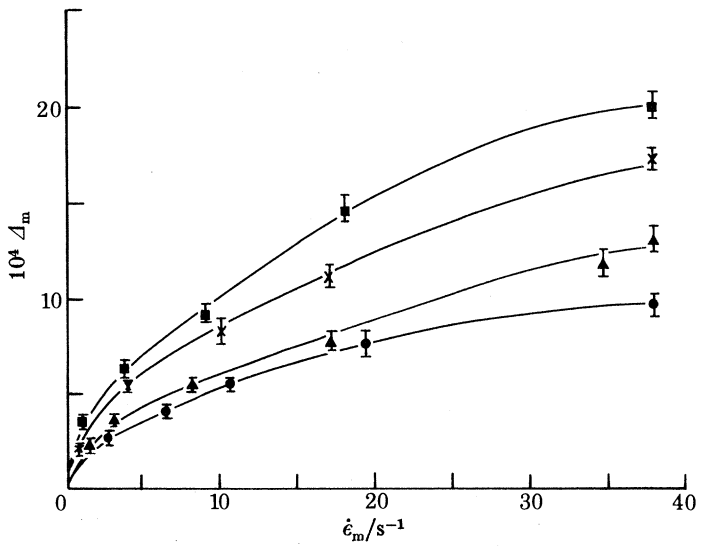

FIGURE 12. Maximum birefringence at throat Δ_m, as a function of entrance velocity gradient $\dot{\epsilon}_m$ and T for HDPE 006; ●, T = 190 °C; ▲, 170 °C; ×, 150 °C; ■, 144 °C.

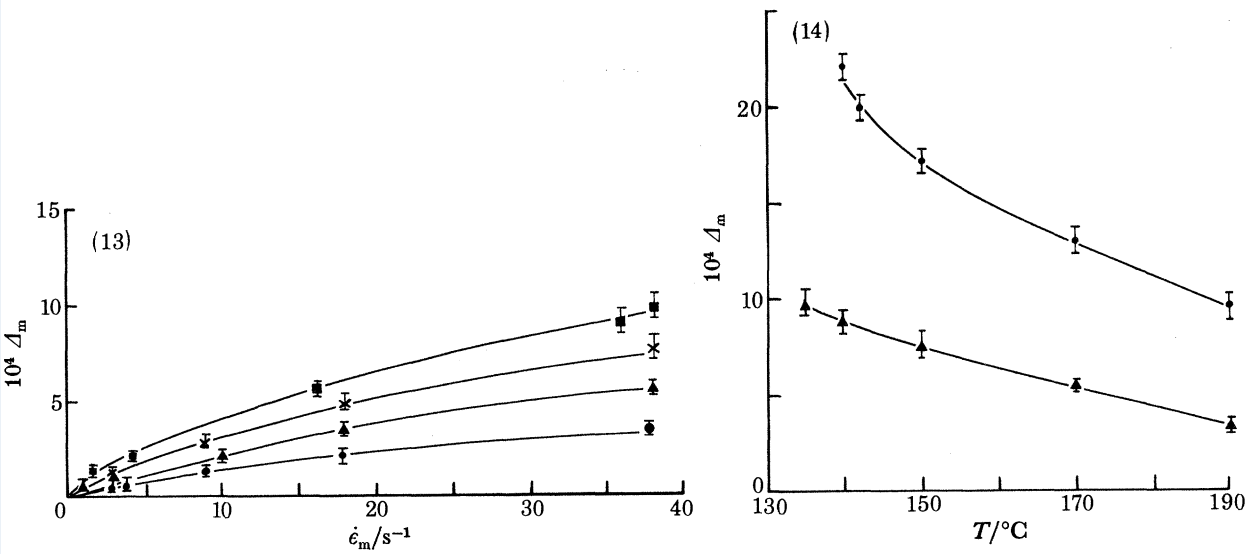

FIGURE 13. Maximum birefringence at throat, Δ_m, as a function of entrance velocity gradient $\dot{\epsilon}_m$ and T for HDPE 50 ($\bar{M}_n = 9\times10^3$, $\bar{M}_w = 9\times10^4$): ●, $T = 190\,°C$; ▲, 170 °C; ×, 150 °C; ■, 144 °C.

FIGURE 14. Maximum birefringence, Δ_m, as a function of temperature for, ●, HDPE 006 ($\bar{M}_w = 13\times10^4$) and, ▲, HDPE 50 ($\bar{M}_w = 9\times10^4$) at $\dot{\epsilon}_m = 38\,s^{-1}$.

given flowrate, Δ_m increases with decreasing temperature and increases with increasing molecular weight. The temperature dependence of Δ_m is more clearly shown in figure 14. There is an essentially linear dependence on temperature with the suggestion that at temperatures close to the melting point the effect of temperature becomes greater.

3.3. *Flow birefringence within the slit*

The changes in birefringence occurring within the slit can easily be followed by referring to, say, figure 8*b*. Across the throat at the entrance of the slit the level of molecular orientation is nearly uniform. As the polymer flows within the slit there is a rearrangement of the stress pattern due to the changes in the velocity field. Near the walls of the slit the stress levels are essentially maintained by the simple shearing velocity gradient, while on moving away from the walls the magnitude of the simple shearing velocity gradient decreases, and the stress levels correspondingly decrease. On the centre line within the slit both longitudinal and shearing velocity gradients are zero and consequently the polymer is free to relax. We therefore see a progressive decay in birefringence along the centre line within the slit region.

Near the walls of the slit it can be seen in all the photographs that the fringes rapidly become parallel to the walls, indicating when this has happened that the stress levels are no longer changing with position along the slit and a steady-state, time-independent equilibrium shear stress at the wall has been established. This is not so in the central region where the polymer is relaxing over the whole observed depth of the slit.

In figure 15 we compare the birefringence observed in the simple shearing flow at the walls of the slit with the birefringence observed at the throat. The data are presented as functions of the simple shearing velocity gradient $\dot{\gamma}$ acting at the wall and the longitudinal velocity gradient $\dot{\epsilon}_m$ acting at the throat.

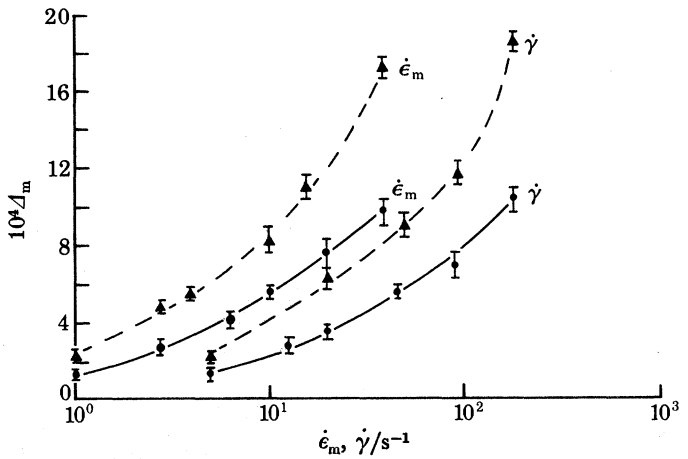

FIGURE 15. Maximum birefringence at throat and slit wall as a function of $\dot{\epsilon}_m$ and maximum shear rate at wall $\dot{\gamma}$ respectively for HDPE 006: ▲, $T = 150$ °C; ●, $T = 190$ °C.

3.4. *Centre-line relaxation*

We have examined in some detail the decay in birefringence along the centre line as this gives very useful information concerning the free relaxation of the polymer that has been oriented in the entrance region. In the photographs we observe a decay of birefringence as a function of position within the slit along the centre line. If we assume a parabolic profile to the flow, the centre-line velocity is 1.5 times the mean velocity $\overline{V}$ within the slit. Thus, if we assume the velocity is uniform along the centre line, it is straightforward to plot the decay of birefringence as a function of time. Figures 16–20 show the decay of birefringence along the centre line as a function of time and at different temperatures, flow rate and molecular weight.

The general feature of the decay is that an initial 'short-time' relaxation generally occurs in the time scale that can be observed within the slit. There then follows a 'long-time' relaxation with a time scale very much greater than the typical transit time of the polymer through the duct.

To determine quantitatively the influence of the various parameters upon the relaxation process, the analysis was divided, as a first approximation, into two time scales: an initial exponential short-time relaxation τ_i where $0 < \tau_i < 0.05$ s and a residual long-time relaxation τ_r where $\tau_r \gg 0.05$ s. In addition we say that the centre-line birefringence in the region we observe is the sum of two contributions given by

$$\Delta_t = \Delta_0 \exp(-t/\tau) + \Delta_r, \tag{4}$$

where Δ_t is the birefringence at time t, Δ_0 is the initial birefringence contribution given by $\Delta_m - \Delta_r$ and Δ_r is the residual birefringence taken as the total birefringence at the longest observed time and indicated by the dashed line on some of the curves in figures 16–19.

The result of analysing the data on this basis is shown in figures 21 and 22. For any given condition of flow the initial relaxation was found to be described reasonably well by a single exponential. As can be seen in figures 21 and 22, surprisingly, it was found for this data that the initial relaxation time was independent of temperature. The values that we obtain for the initial relaxation time under different conditions are tabulated in table 2.

We are unable to measure the value of the long relaxation time but we are able to measure the relative amounts of birefringence that correspond to both initial and residue birefringence

PHILOSOPHICAL TRANSACTIONS OF THE ROYAL SOCIETY A MATHEMATICAL, PHYSICAL & ENGINEERING SCIENCES

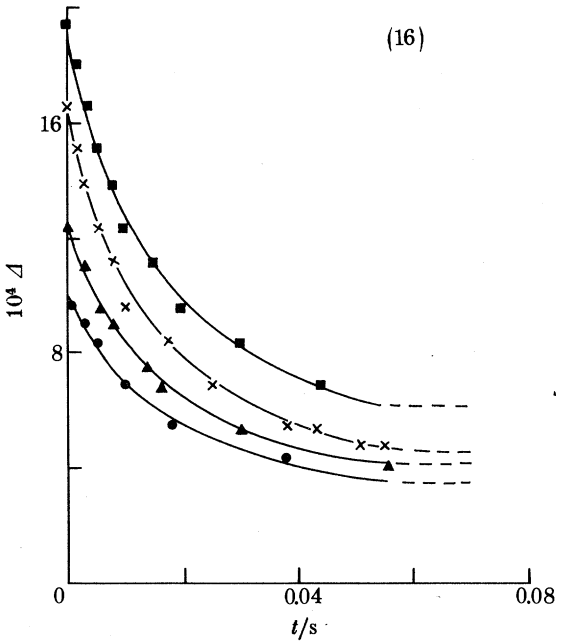

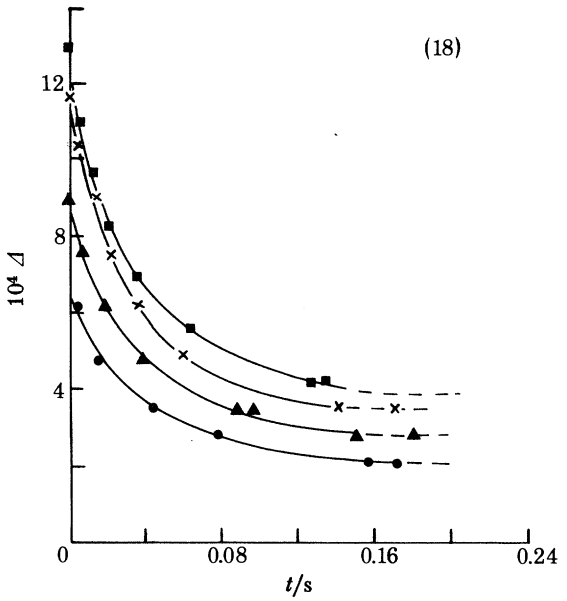

FIGURE 16. Centre-line birefringence decay profiles within slit section at different temperatures for HDPE 006 with $\dot{\epsilon}_m = 38\ s^{-1}$: ●, $T = 190\,°C$; ▲, 170 °C; ×, 150 °C; ■, 144 °C.

FIGURE 18. Centre-line birefringence decay profiles within slit for HDPE 006 with $\dot{\epsilon}_m = 19\ s^{-1}$: ●, $T = 190\,°C$; ▲, 170 °C; ×, 150 °C; ■, 144 °C.

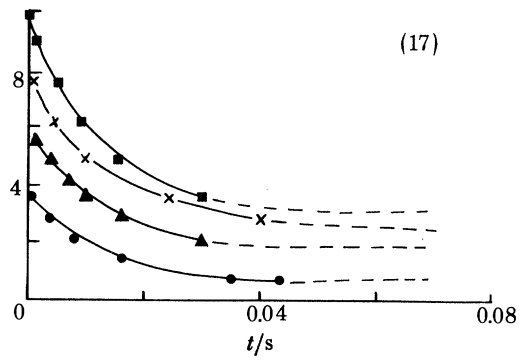

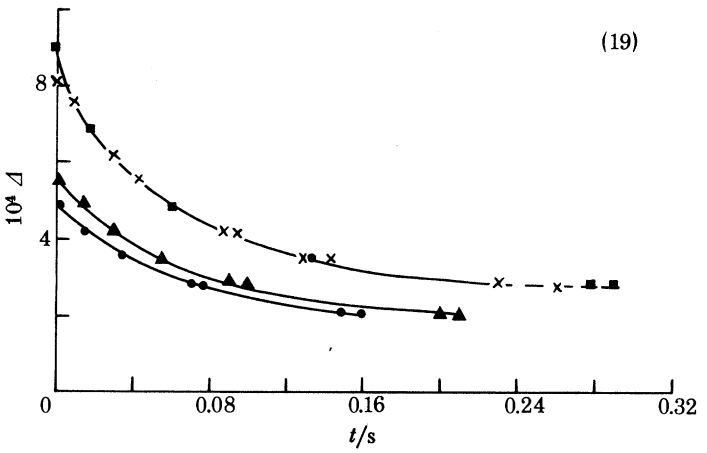

FIGURE 17. Centre-line birefringence decay profiles within slit for HDPE 50 with $\dot{\epsilon}_m = 38\ s^{-1}$: ●, $T = 190\,°C$; ▲, 170 °C; ×, 150 °C; ■, 144 °C.

FIGURE 19. Centre-line birefringence decay profiles within slit for HDPE 006 with $\dot{\epsilon}_m = 9\ s^{-1}$: ●, $T = 190\,°C$; ▲, 170 °C; ×, 150 °C; ■, 144 °C.

and these correspond to Δ_0 and Δ_r respectively. The two quantities Δ_0 and Δ_r are plotted as a function of $\dot{\epsilon}_m$ and T in figures 23 and 24.

The results presented so far clearly demonstrate the level of complexity associated with the flow behaviour of molten polymers. In particular we find that along the centre line of the slit where no velocity gradients are active the relaxation behaviour depends on factors such as $\dot{\epsilon}_m$, the entrance velocity gradient, and T, the absolute temperature. At this stage in the paper

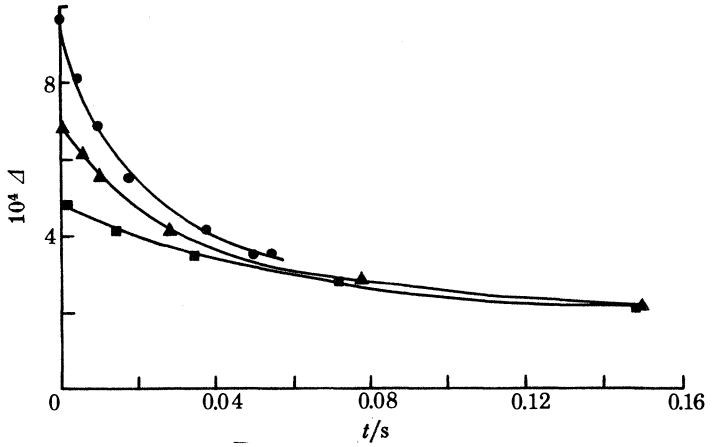

FIGURE 20. Centre-line birefringence decay profiles within slit at different values of $\dot{\epsilon}_m$ for HDPE 006 at 190 °C: ●, $\dot{\epsilon}_m$ = 38 s^{-1}; ▲, 18 s^{-1}; ■, 9 s^{-1}.

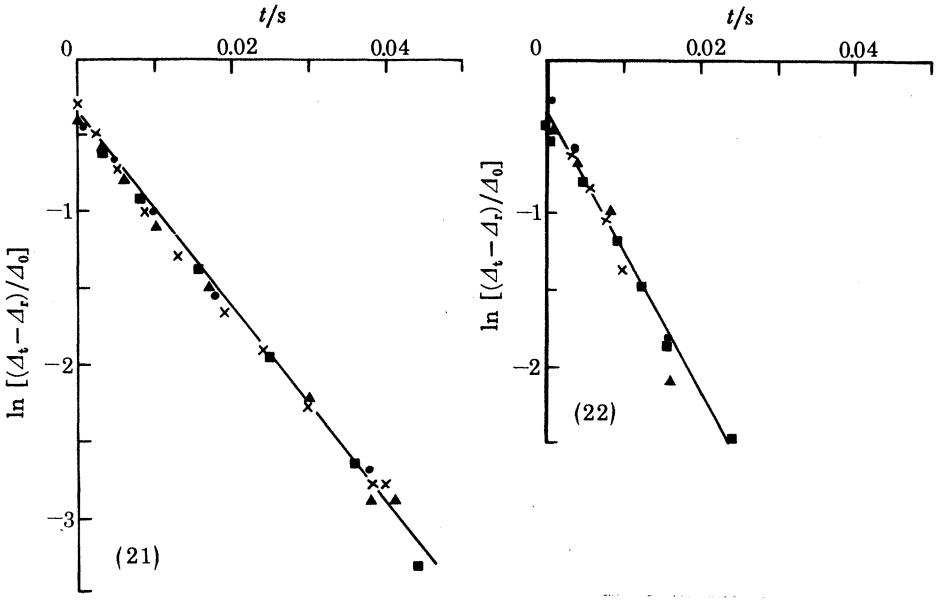

FIGURE 21. Plot of $\ln[(\Delta_t-\Delta_r)/\Delta_0]$ as a function of t for HDPE 006: ●, T = 190 °C; ▲, 170 °C; ×, 150 °C; ■, 144 °C.

FIGURE 22. Plot of $\ln[(\Delta_t-\Delta_r)/\Delta_0]$ as a function of t for HDPE 50: ●, T = 190 °C; ▲, 170 °C; ×, 150 °C; ■, 144 °C.

we have demonstrated the existence of two contributions to the birefringence and hence the relaxation process. Both contributions depend differently on $\dot{\epsilon}_m$ and T and both depend on the molecular weight distribution of the polymer.

3.5. *The effect of entrance geometry*

The quantitative results reported in this paper are limited to the one entrance geometry previously described. We believe the entrance geometry is critical in that it controls both the strain and velocity gradient history of the polymer before it enters the slit. This is particularly important in our case because the polymer starts from an essentially quiescent 'equilibrium

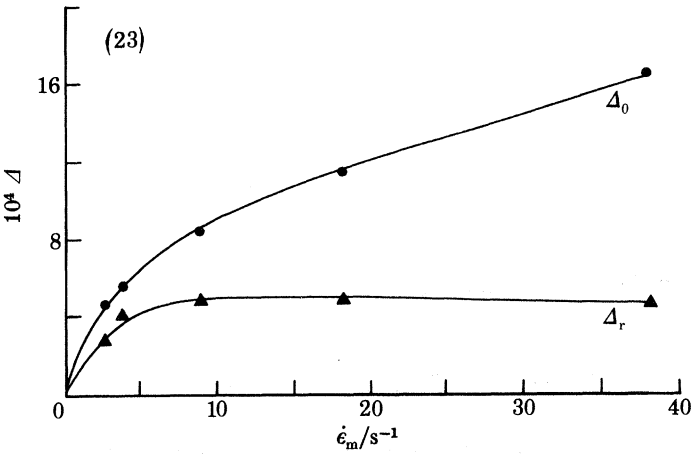

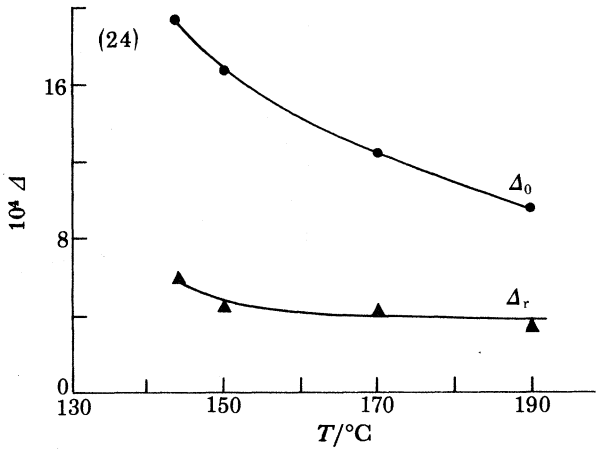

FIGURE 23. Plot of Δ_0 and Δ_r as a function of $\dot{\epsilon}_m$ for HDPE 006 at 150 °C.

FIGURE 24. Plot of Δ_0 and Δ_r as a function of T for HDPE 006 with $\dot{\epsilon}_m = 38\ s^{-1}$.

state' within the barrel of the rheometer and the only significant strain history the material receives up to the throat is in the entrance region of the duct. If the material had been fed to the duct by a screw extruder, for example, the state of the melt at the entrance region could be very different owing to the complex shear history that the material would have had. Under these conditions we would threfore expect observations of subsequent behaviour in the slit to be significantly different from those that we have observed; in particular we propose that much of our observed long time relaxation behaviour would not occur.

To demonstrate qualitatively the effect that entrance geometry can have on overall birefringence patterns, we include one series of photographs for a 'trumpet shaped' entrance region. In this duct the cross section of the entrance region was smoothly reduced from 15×7.6 mm to 1×7.6 mm over a distance of 20 mm. Figure 25 (plate 2) shows a series of flow birefringence photographs of the observed birefringence for this geometry and should be directly compared with figure 8 for the semicircular entrance geometry. For the trumpet shape the shearing at the side walls dominates the flow, and stresses develop from the side walls in a similar way to a fluid boundary layer growing on a curved or flat plate. The magnitude of the extensional velocity gradient in the entrance region is significantly lower than the shear velocity gradient at the walls and hence the levels of orientation along the centre line lag behind the levels of orientation on the side walls. Consequently when the throat is reached centre-line relaxation does not occur to the same extent as previously, owing to the reduced amount of oriented material on the centre line. At the throat, levels of orientation are highest near the walls and are low in the central region. The development with position of the birefringence on the side walls of the trumpet duct would in our opinion give useful information on the time-dependent birefringence of polymers in simple shearing flow. We have, however, not explored this aspect further.

3.6. *Instabilities*

In most commercial processing of molten polymers it is usually desirable to maximize the throughput of any device. For a given system this can often be achieved by using low molecular weight material, invariably, however, at the penalty of poor final properties of the product.

For a given material and molecular weight distribution the maximum throughput is often set by the onset of instabilities in the flow, which with extrusions lead to an irregularly shaped extrudate. The subject of instabilities has received detailed attention by, amongst others, Tordella (1969) and Pearson (1976).

We generally made experimental observations in régimes where the flow was steady and free from instabilities. However, we did on several occasions observe systematic unstable flow behaviour. The onset of these instabilities can depend on unexpected factors such as the amount of polymer in the feed barrel and the barrel's overall shape, in addition to expected factors such as temperature and flow rate. In this paper we report qualitatively the form of two characteristic instabilities that we observed.

Figure 26 (plate 3) shows the typical unstable flow seen for HDPE. With increasing flow rate we noticed that oscillations within the flow emanated from regions close to the throat of the duct. Initially these oscillations were localized at the throat region. However, at higher flow rates they extended to the whole field of view. The stress levels were then seen to oscillate between two levels with a frequency of about 1–5 Hz. Figure 26 shows the two levels. In both cases the overall birefringence pattern is similar in form to the steady-state pattern observed at lower flow rates.

Figure 27 (plate 4) shows a sequence of birefringence patterns observed for a polypropylene copolymer. These photographs have several striking features, in particular the W fringes that can be seen within the slit. Figures 27*a–c* show the steady-state flows at different volumetric flow rates. In these pictures the development of W fringes can be clearly seen. We interpret these W fringes as indicating that in the region where the W is observed downstream of the throat the maximum orientation and velocity gradient exist away from the walls approximately half way between the walls and the centre line. This rather surprising result has recently been predicted by Perrara & Strauss (1979) from numerical analysis of an 'Oldroyd four constant' model flowing into a slit die. Our tentative physical interpretation of this observation is that this particular grade of polypropylene is very 'elastic' and reluctant to be deformed in extensional flows. Thus the material, taking the path of least resistance, prefers to channel around the edges of the duct and be sheared rather than flow near the centre line in the entrance region where the flow is dominantly extensional. The flow in the entrance region near the

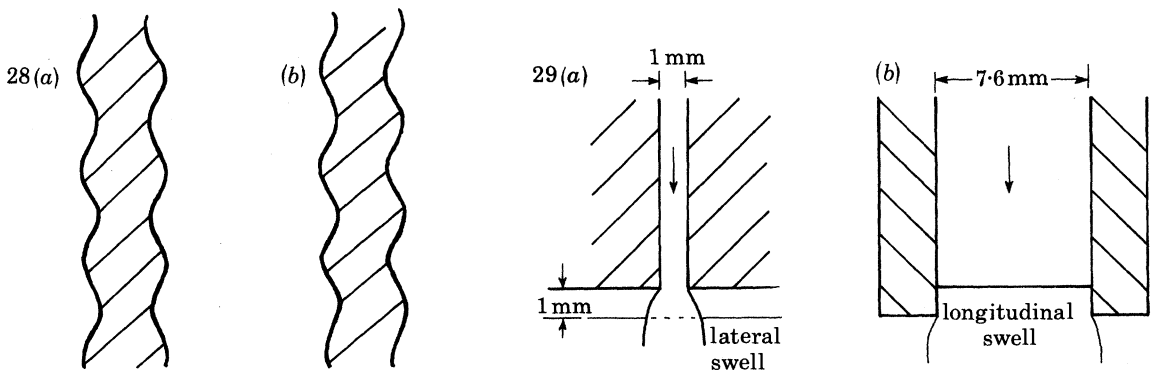

FIGURE 28. Schematic diagram of extrusion profiles obtained under conditions given by (*a*) figure 26 and (*b*) figures 27*d–f*.

FIGURE 29. Schematic diagram of geometrical arrangement at slit exit: (*a*) front elevation; (*b*) side elevation.

centre line becomes effectively blocked and the polymer channels around either side. A similar effect would occur if an obstruction was symmetrically placed upstream in the entrance region.

The view that the flow channels preferentially around the sides of the ducts is supported by the form of instabilities observed in figures 27*d–f*. At an increased flow rate the time sequence shows the manner in which the oscillations occur. Again the oscillations occur at a frequency of about 1–5 Hz but in this case the birefringence pattern is asymmetrical with the flow alternately channelling down either side of the duct in an oscillatory manner. In figure 27*d* the W is deeper on the left-hand side and the flow is channelling on that side of the duct.

The profiles of the polyethylene and polypropylene extrudates obtained under the conditions of figure 26 and 27*d–f* respectively are shown in figure 28.

3.7. *Die swell and flow birefringence at the exit region*

Our final series of experimental observations concerns behaviour at the exit of the duct where the polymer emerges from the slit into free space. The parameter most commonly measured to characterize the overall behaviour is that of die swell χ defined as the ratio of the sectional diameter of the final extrudate to the sectional diameter of the orifice from which the material emerged.

It has been established by several workers that die swell of molten polymers decreases with increasing length/diameter (L/D) ratio of the parallel section of the duct (see for example Middleman 1977; Huang & White 1980). In view of the flow birefringence photographs of figure 8 we initially proposed this result as being due to centre-line relaxation. If the L/D ratio was very small, material in the central region of the duct would not have time to relax within the duct and the final relaxation of stresses on leaving the duct would cause a large die swell. If a large L/D was used, material in the central region of the duct would have time to relax partially or completely within the parallel section of the duct, thus producing a final lower die swell when the material emerged at the exit. While this argument is certainly a significant factor in explaining die swell, we discovered for the generally high molecular weight polymers we examined that the situation requires a more elaborate explanation to describe all our findings. At this stage we also note that other workers (Han & Kim 1971; Huang & White 1980) have established that die swell depends on die-entrance geometry. In the series of experiments to be reported we have chosen not to vary this parameter while acknowledging that it will certainly influence overall behaviour.

When the molten polymer emerges from the slit, a swelling occurs both laterally in the plane containing the 1 mm slit width and longitudinally in the plane containing the 7.6 mm slit depth. If the flow was entirely two-dimensional there would be no longitudinal swelling. However, we find that for our 1 mm × 7.6 mm slit the longitudinal swell is small but of sufficient magnitude to produce a curved surface as the melt emerges from the slit. This causes severe distortion of the light as it is refracted at the polymer/air interface, making optical interpretation of the flow birefringence difficult. To overcome this problem we lowered the two faces of the glass windows by 1 mm below the bottom of the slit walls; the situation is shown schematically in figure 29. By doing this we have produced a 'constrained die swell', in that the polymer is free to swell laterally but not longitudinally initially.

The time-dependent behaviour of die swell is in our opinion an important and neglected parameter. We have made some attempts to measure this behaviour by recording two die-swell measurements at different times. The first 'initial die swell' χ_i was measured as the lateral

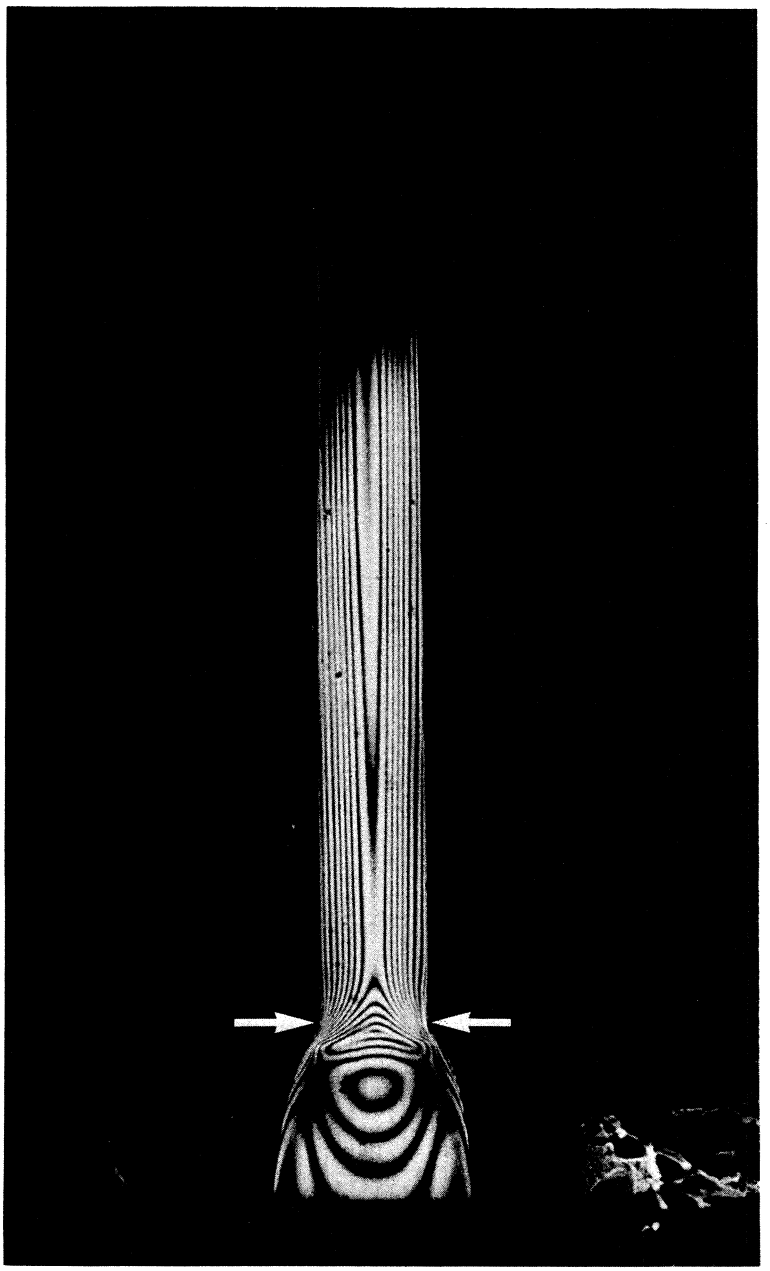

FIGURE 30. Flow birefringence at slit exit for HDPE 02–55 at 210 °C with $L/D = 16$ mm/1 mm, $\bar{v} = 639$ mm³/s. Polars are crossed at 45°.

(*Facing p.* 466)

PHILOSOPHICAL TRANSACTIONS OF THE ROYAL SOCIETY A MATHEMATICAL, PHYSICAL & ENGINEERING SCIENCES

PHILOSOPHICAL TRANSACTIONS OF THE ROYAL SOCIETY A MATHEMATICAL, PHYSICAL & ENGINEERING SCIENCES

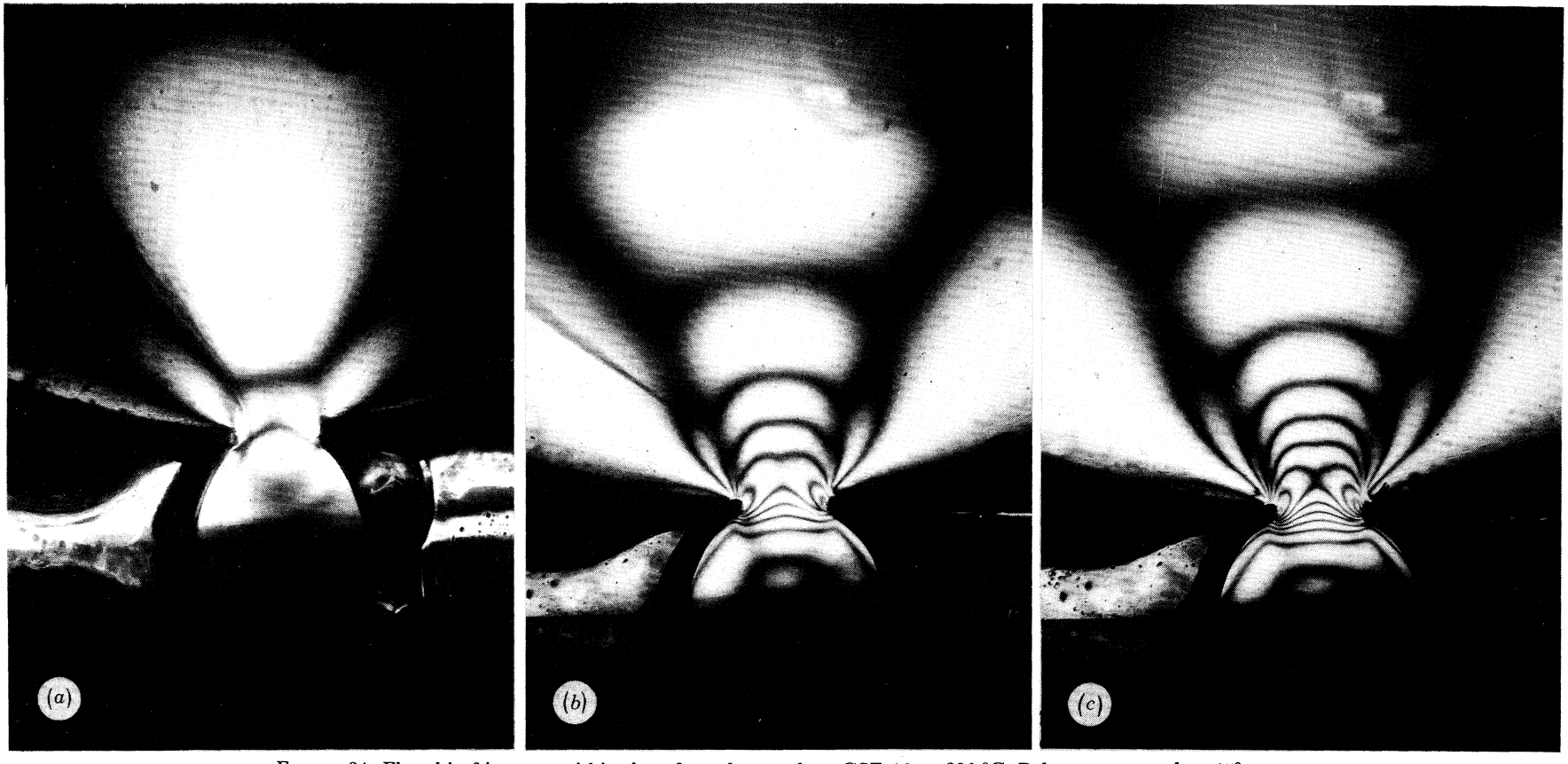

FIGURE 31. Flow birefringence within duct for polypropylene GSE-16 at 230 °C. Polars are crossed at 45°.

(*a*)–(*c*) L/D = 0.1 mm/l mm; (*a*) $\bar{v}$ = 63 mm³/s, (*b*) 318 mm³/s, (*c*) 574 mm³/s.
(*d*)–(*f*) L/D = 2.3 mm/l mm; (*d*) $\bar{v}$ = 63 mm³/s, (*e*) 318 mm³/s, (*f*) 574 mm³/s.
(*g*)–(*i*) L/D = 8 mm/l mm; (*g*) $\bar{v}$ = 63 mm³/s, (*h*) 318 mm³/s, (*i*) 574 mm³/s.
(*j*)–(*l*) L/D = 16 mm/l mm; (*j*) $\bar{v}$ = 63 mm³/s, (*k*) 318 mm³/s, (*l*) 574 mm³/s.

Parts (*d*)–(*l*) appear on plates 7 and 8.

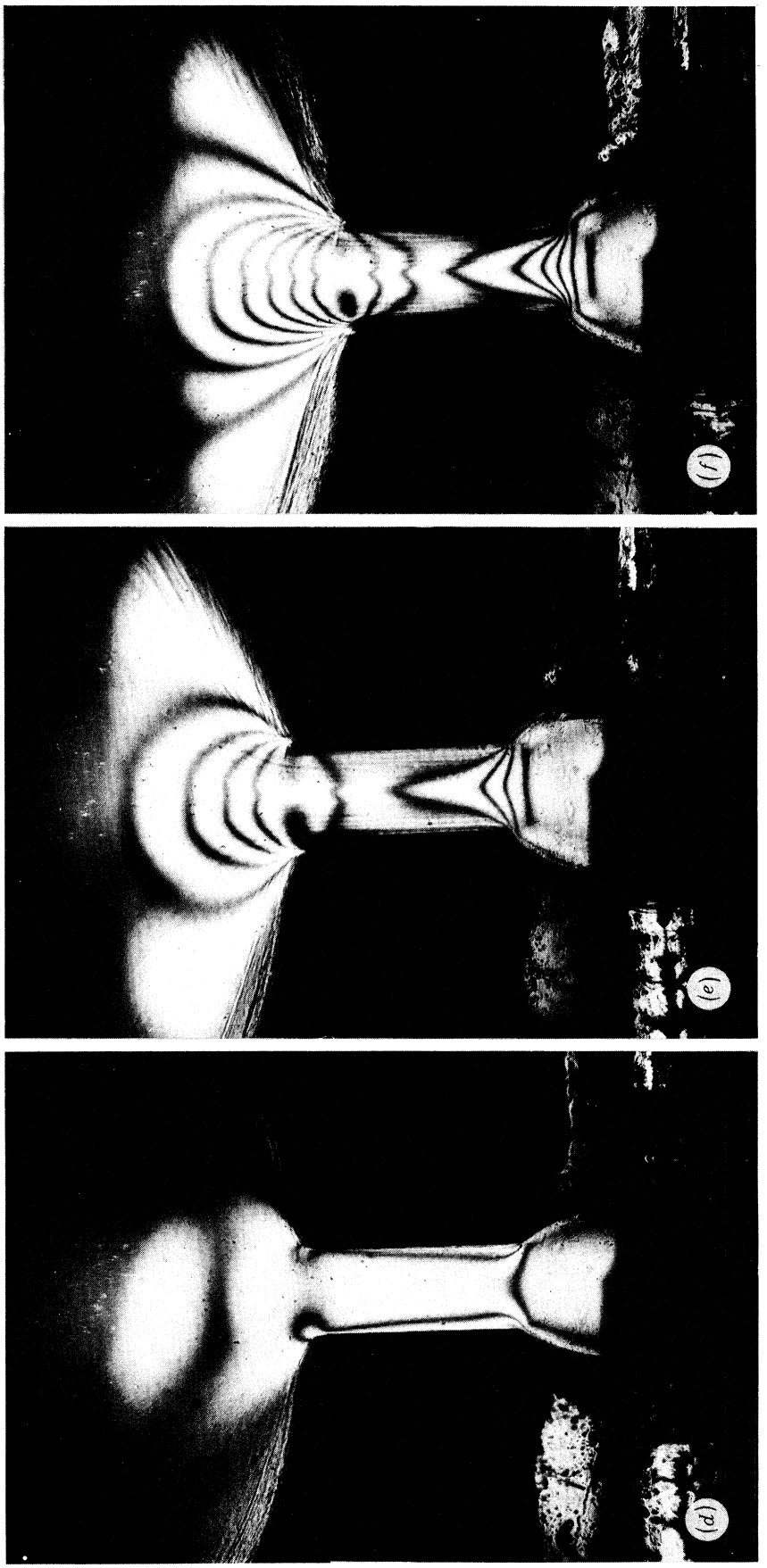

FIGURE 31 (*d*)–(*f*). For description see plate 6.

PHILOSOPHICAL TRANSACTIONS OF THE ROYAL SOCIETY A MATHEMATICAL, PHYSICAL & ENGINEERING SCIENCES

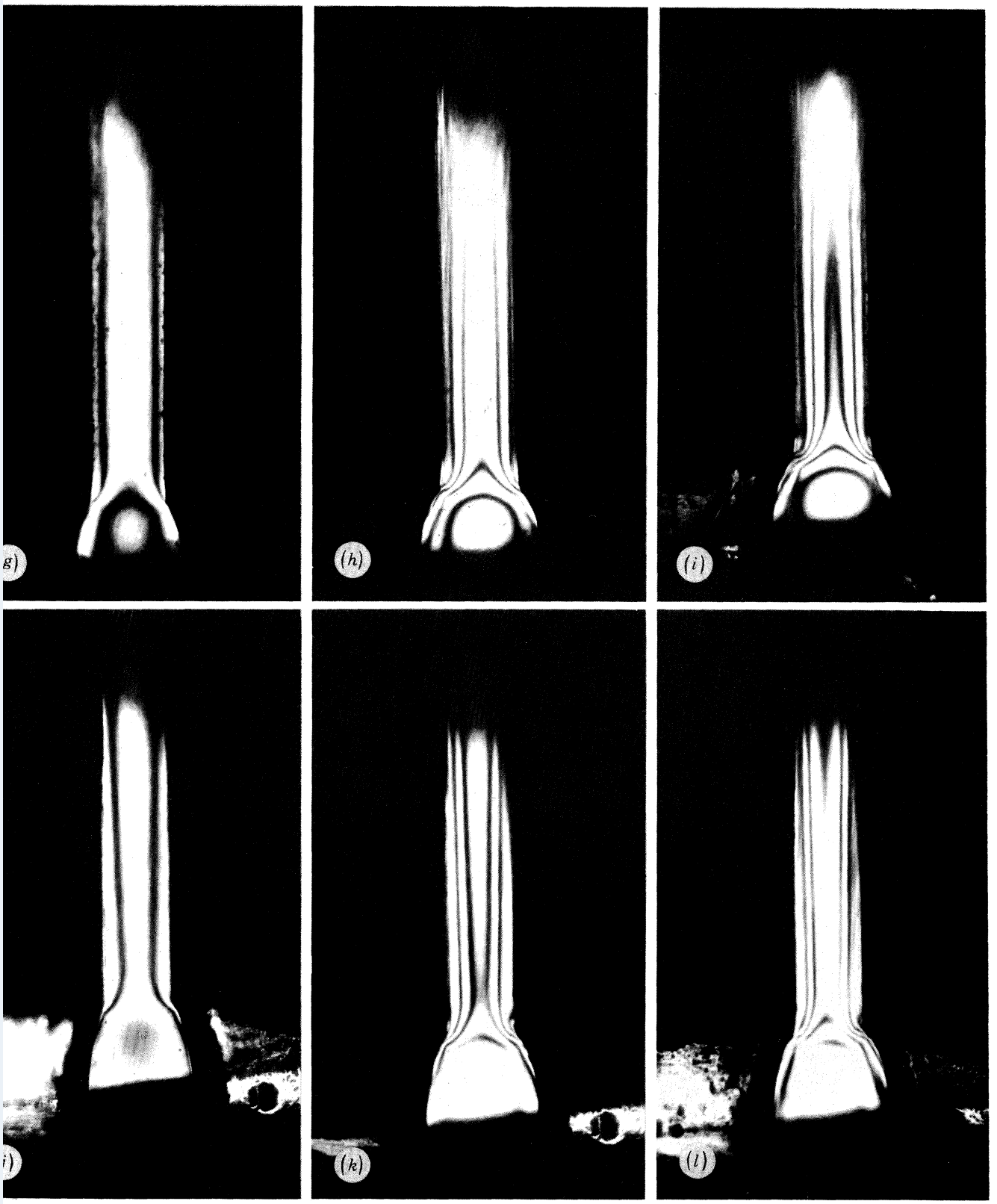

FIGURE 31 (*g*)–(*l*). For description see plate 6.

PHILOSOPHICAL TRANSACTIONS OF THE ROYAL SOCIETY A MATHEMATICAL, PHYSICAL & ENGINEERING SCIENCES

swell optically observed when the polymer was at an arbitrary distance of 1 mm below the slit and at the bottom of the polished face of the glass window. Subsequently the polymer would leave the constant-temperature region, cool, and eventually solidify. The lateral swell of the sample at this point had little meaning because the material had crystallized and also possessed frozen-in strain. To measure what we shall term ultimate die swell χ_∞, solidified sections of the extrudate were heated in an oven for at least 1 h at a temperature that was close to or up to 5 °C above the melting range of the polymer. In this way the polymer was allowed to relax completely, allowing the final lateral swell to be measured.

We know of two previously published birefringence photographs showing the flow of molten polymer at a slit exit, namely those of Mori & Funatsu(1973) and Han (1976). Unfortunately these photographs do not show the same general trends reported in this paper. We are confident in our results and therefore conclude that either the different polymer, experimental conditions or optical effect due to stray reflexions and/or curvature at the melt air interface lead to the differences. From our own early experiences we suspect the optical effects.

Figure 30 (plate 5) shows a representative flow birefringence photograph of polypropylene flowing out of a slit with an L/D ratio of 16/1. The slit exit has been marked by white arrows and the bottom of the glass window is clearly seen below the exit. Because of the curvature of the melt no further birefringence is seen below the glass window although the polymer continues to swell slightly before forming the final solid extrudate.

Within the slit and well upstream of the exit we conclude that steady shearing on and near the side walls occurs as the retardation bands in this region are very nearly parallel to the walls of the slit. Along the centre line, the retardation is still slowly decreasing owing to the centre-line relaxation discussed in §3.4. The last observation demonstrates the initially rather surprising result that within the slit the flow is not truly viscometric even for an L/D ratio of 16/1. The main reason for the non-viscometric state is the presence of the 'residue' birefringence, which has a relaxation time very much greater than the residence time of the polymer through the duct. As shown previously the amount of residue birefringence increases with increasing molecular weight and decreasing temperature.

About 1 mm upstream from the slit exit the birefringence pattern changes and there is a considerable modification of the stress pattern before the exit is reached. This is an important result as most theories concerned with die swell of viscoelastic materials assume that the flow is viscometric up to the exit (see for example the review by Boger & Denn (1980). The general form of the retardation bands indicates that the stress rapidly diminishes in the central region as the exit is approached and very high stress concentrations occur at the slit edges. The subsequent modification of stresses downstream of the exit is complex.

The effect of variable L/D ratios is shown in figure 31 (plates 6–8). Here it can be seen that for L/D ratios of less than say 5/1 the upstream birefringence pattern is intimately related to the downstream behaviour.

To follow the stress or birefringence pattern within and out of a duct we chose to analyse in detail a duct with an L/D ratio of 2.5. Figure 32 shows a schematic diagram of the duct together with the streamlines of the flow drawn as dotted lines. Within the duct the direction of the largest-magnitude principal optic and stress axis is shown by dashes. The magnitude of the local principal stress difference is indicated by the length of the dashes. The direction of the dash indicates the local overall direction in which the polymer chains are oriented and the length of the dash indicates the extent to which the chains are stretched. Information on

PHILOSOPHICAL TRANSACTIONS OF THE ROYAL SOCIETY A MATHEMATICAL, PHYSICAL & ENGINEERING SCIENCES

both direction and magnitude of the principal stress difference can be readily obtained from a series of flow birefringence photographs taken with the polars set at different angles to the axis of the duct.

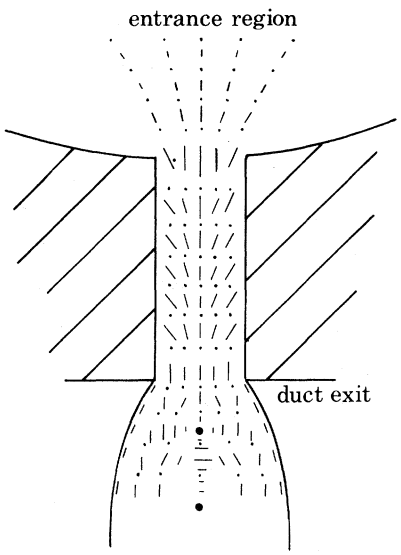

FIGURE 32. Schematic form of flow within duct. Dots correspond to streamline trajectory. Direction of dashes corresponds to the direction of the positive principal stress and magnitude of dashes corresponds to the relative magnitude of the principal stress difference.

Within the entrance region of the duct the stress builds up to a maximum at the throat of the duct and the direction of the principal stress axis is essentially parallel to the streamlines. Within the slit there is a rapid adjustment to accommodate the shearing at the side walls. Stress levels are generally maintained near the side walls but the principal stress axis now takes up a characteristic angle with respect to the stream lines. In the centre of the duct the principal stress axis is parallel to the centre line. However, centre-line relaxation takes place and consequently the magnitude of the principal stress difference progressively decreases within the slit.

If the fluid was Newtonian, in the simple shearing regions near the duct walls, the direction of the principal stress axis would be at 45° to the direction of flow. As the polymer is non-Newtonian this angle is less and, for the flow rates we typically work with, would range from a few degrees to 45° at very low flow rates.

When the exit is approached we have discovered that in all cases studied the direction of the principal axis adjusts to become parallel to the streamlines at the exit. This adjustment occurs over a distance upstream from the exit of about 1–2 mm. In our opinion the observation concerning the direction of the principal stress axis at the axis has significance particularly in relation to correct boundary conditions for the mathematical modelling of die swell.

The magnitude of the principal stress difference varies across the exit. In general it would be largest at the walls and progressively decrease towards the centre line of the slit. The effect of increasing L/D is apparent at the exit as the magnitude of the principal stress difference at the walls of the duct is not significantly affected by L/D. The magnitude of the principal stress

difference at the centre of the duct will decrease with increasing L/D owing to centre-line relaxation.

When the polymer leaves the duct a complex rearrangement of stresses takes place. Fluid elements in the outer regions away from the centre line are initially accelerated and stretched. Fluid in the central region decelerates and we observe under all conditions an area about the centre line where the principal stress difference becomes zero. We term this node a 'neutral zone'. Along the centre line further downstream of the neutral zone, further stretching often takes place before eventual relaxation occurs.

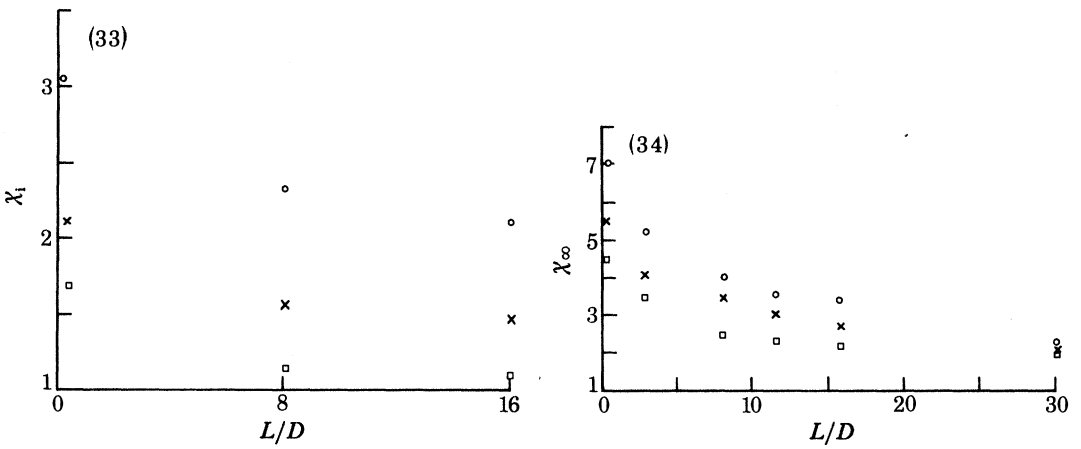

FIGURE 33. Plot of initial die swell χ_i as a function of L/D for polypropylene GSE 16 at 230 °C; ○, $\bar{v} = 1000$ mm³/s; ×, 476; □, 159.

FIGURE 34. Plot of ultimate die swell χ_∞ as a function of L/D for polypropylene GSE 16 at 230 °C. ○, $\bar{v} = 1000$ mm³/s; ×, 476, □, 159.

With the exception of the neutral zone we are unable to make any general comments concerning the stress distribution pattern immediately downstream of the exit because we have found that the details of the pattern are sensitive to all our major variables such as flow rate, polymer and molecular weight as well as the exact downstream conditions of the extrudate.

Our final experimental results relate to the observed values for our initial χ_i and ultimate χ_∞ die swell. Our primary interest is the way in which χ_i and χ_∞ vary with L/D. Figure 33 shows for polypropylene the manner in which χ_i varies with L/D at three different flow rates. The swelling was measured directly from photographs of the type shown in figure 31. The die swell decreases with L/D; however, the maximum value of χ_i we have observed for any polymer never exceeded 5 and typically is much less. The ultimate die swell obtained after complete relaxation of the extrudate is shown as a function of L/D in figure 34. This graph shows some remarkably high die swells when the L/D is low. In our discussion we are particularly interested in the relative contribution of the initial and ultimate die swell as a function of L/D and, in anticipation of that, plot in figure 35 the ratio χ_i/χ_∞ as a function of L/D.

We have stated before that owing to experimental limitations our slit is only 7.6×1 mm. The swelling reported in figures 33 and 34 relates to lateral swelling in the plane containing the 1 mm width. The longitudinal swelling is much less and only weakly dependent on L/D. Typical values of the ultimate longitudinal swelling are shown in figure 36.

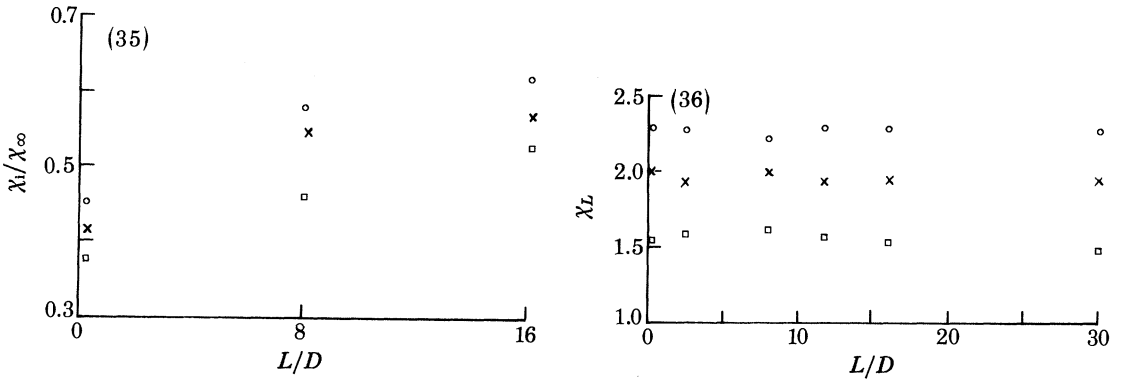

FIGURE 35. Plot of χ_i/χ_∞ as a function of L/D for polypropylene GSE 16 at 230 °C: ○, $\bar{v}$ = 1000 mm³/s; ×, 476; □, 159.

FIGURE 36. Plot of longitudinal die swell, χ_L, as a function of L/D for polypropylene GSE 16 at 230 °C; ○, $\bar{v}$ = 1000 mm³/s; ×, 476; □, 159.

4. Discussion

The flow behaviour of commercial grades of polymer melt flowing into, within and out of ducts is complex, and in our opinion we are at present not able to construct a physical or mathematical model that is capable of describing all the events we have reported. Our objective in this discussion therefore is restricted to giving a semi-quantitative explanation for some of the results that we have recorded and our attention will be mainly directed at behaviour along the centre line of the duct. We choose to discuss first the centre-line relaxation within the slit section of the duct, followed by entrance region effects and finally the behaviour at the slit exit.

4.1. *Centre-line relaxation*

Within the slit section and along the centre line of the duct we have established that both longitudinal and transverse velocity gradients are zero. It is therefore possible to follow along the centre line the free relaxation of birefringence for fluid elements that have previously been stretched by the longitudinal velocity gradient $\dot{\epsilon}_m$ in the entrance region. We have shown that the birefringence decays in a manner given by equation (4):

$$\Delta_t = \Delta_0 \exp(-t/\tau_i) + \Delta_r \ldots,$$

where Δ_t is the birefringence at time t, τ_1 the initial exponential relaxation time, Δ_r the residue birefringence and Δ_0 the initial birefringence contribution given by $\Delta_0 = \Delta_m - \Delta_r$, Δ_m being the maximum birefringence at the throat of the slit.

The values of τ_i obtained as a function of several variables are shown in table 2 and it can be seen that, contrary to possible initial expectations, τ_i is independent of temperature T and only weakly dependent on molecular weight. However, τ_i does depend on the entrance velocity gradient $\dot{\epsilon}_m$. We have also shown that the magnitude of the residue birefringence Δ_r is essentially independent of temperature T and independent of the entrance velocity gradient $\dot{\epsilon}_m$ for $\dot{\epsilon}_m$ greater than about 5 s^{-1}.

To explain this relaxation behaviour and other reported observations, we have found it instructive to consider that the melt behaves as a composite fluid. We envisage that melt consisting of a network of entangled high molecular weight chains embedded in a matrix of lower molecular weight chains. We assign the matrix component to the initial relaxation time, and the network contribution to the residue birefringence.

The matrix component and its associated initial relaxation time behaves in an unexpected way. Normally relaxation times would decrease with increasing temperature and decreasing molecular weight. Our results do not follow this trend and we interpret this finding by concluding that we are measuring the birefringence of a selected fraction of the molecular weight distribution.

Our model assumes that the origin of birefringence arises solely from chain orientation. Thus we exclude form birefringence contributions and contributions due to bond stretching, the latter being ignored because our stresses in the melt are low and usually below 10^6 N/m^2. For the molecules to contribute to the birefringence, the chains must be oriented. However, at present no satisfactory theory appears to exist concerning the way in which velocity fields affect the stretching of chains within a polymer melt. The situation is somewhat better in dilute solution where, for example, several authors have shown that in pure shearing flow, if the condition $\dot{\epsilon}\tau > 1$ is satisfied, the chains will be fully stretched by the flow (Ziabicki 1959; Peterlin 1967; Mackley & Keller 1975), where $\dot{\epsilon}$ is the magnitude of the applied velocity gradient and τ the longest relaxation time of the chain. For our analysis we chose to make the assumption that if $\dot{\epsilon}\tau \geqslant \alpha$ the chains will be influenced by the flow and stretched; if $\dot{\epsilon}\tau < \alpha$ the chains are assumed to remain undeformed. Here α is a variable parameter that on the basis of dilute solution theory may plausibly be expected to vary between about 0.1 and 5. On this basis, for molecules contributing to the matrix component, if $\dot{\epsilon}\tau \geqslant \alpha$, the chains will be deformed and contribute to the birefringence; if $\dot{\epsilon}\tau < \alpha$, the chains will remain undeformed with no birefringence contribution and will be merely convected by the flow. Thus, for the matrix contribution, only molecules with a relaxation time $\tau \geqslant \alpha/\dot{\epsilon}_{\mathrm{m}}$ will be stretched in the entry region and therefore contribute to the birefringence Δ_0 at the throat.

To make a quantitative prediction of the observed initial relaxation times within the slit, it is necessary to know the relaxation time distribution of the polymer. This presents certain difficulties, associated mainly with the use of samples that had broad molecular weight distributions.

Following Blundell & Keller (1968) we assume that the number of chains with a degree of polymerization x is given by the log normal distribution

$$N(x) = \frac{1}{[\sigma(2\pi)^{\frac{1}{2}}]}\frac{1}{[m_1 x^2]}\exp\left\{\frac{-[\ln(\mathrm{m}_1 x) - \ln(m_1 x')]^2}{2\sigma^2}\right\} \tag{5}$$

where σ and x' are constants and m_1 the molecular mass of each repeat unit ($CH_2 - CH_2 = 28$). Using equation (5) and the definitions of number and weight average molecular weights, it is possible either by direct integration (Wesslau 1956) or by numerical integration to determine the constants σ and x'. For the molecular weight distributions used in this paper these analytical results are shown in table 1.

To utilize the stretch condition $\tau \geqslant \alpha/\dot{\epsilon}_{\mathrm{m}}$ we must arrive at an expression for τ as a function of temperature T and degree of polymerization x. We chose

$$\tau = C_1 x/T, \tag{6}$$

TABLE 1. LOG NORMAL DISTRIBUTION PARAMETERS σ AND x' GIVEN IN EQUATION (5) COMPUTED FOR VALUES OF $\bar{M}_n$ AND $\bar{M}_w$ USED IN PAPER

$\bar{M}_n$	$\bar{M}_w$	σ	x'
20×10^3	13×10^4	1.37	1820
9×10^3	9×10^4	1.52	1008
14×10^3	65×10^4	1.24	1064

where C_1 is a constant. This choice is based on earlier considerations (Mackley & Keller 1975) on the way τ may plausibly be expected to vary with x and T. Combining equations (5) and (6) yields

$$N(\tau) = \frac{1}{[\sigma(2\pi)^{\frac{1}{2}}]} \frac{C_1^2}{[\tau^2 T^2 m_1^2]} \exp\left[-\left\{\ln\left(\frac{m_1 T \tau}{C_1}\right) - \ln(m_1 x')\right\}^2 \Big/ 2\sigma^2\right], \tag{7}$$

where $N(\tau)$ is the number of molecules with relaxation time τ.

We now further assume that the only molecules to take part in the initial relaxation along the centre line within the slit are the molecules that have been stretched in the entrance region by the pure shearing velocity gradient $\dot{\epsilon}_m$. Our experimental observations will record the mean relaxation time τ_m of the stretched molecules given by

$$\tau_m = \int_{\alpha/\dot{\epsilon}_m}^{\infty} \tau N(\tau)\, d\tau \Big/ \int_{\alpha/\dot{\epsilon}_m}^{\infty} N(\tau)\, d\tau. \tag{8}$$

On substituting equation (7) into (8) it is then possible to numerically integrate (8) to give a predicted value of τ_m. Parameters σ, x' and m are fixed by the polymer under examination and $\dot{\epsilon}_m$ and T are controlled by the experimental conditions. Parameters C_1 and α are variables that must be chosen. To compare the model with the experimental results given in table 2 we have selected $\alpha = 0.25$ and have chosen a value of C_1 that gives agreement between our predicted and observed results of τ for the condition. $T = 144\,^{\circ}\mathrm{C}$, $\dot{\epsilon}_m = 38\ \mathrm{s}^{-1}$, $\bar{M} = 20000$, $\bar{M}_w = 130000$. This gives

$$C_1 = 0.006\ \mathrm{s}\ ^{\circ}\mathrm{C}. \tag{6}$$

With $C_1 = 0.006$ and $\alpha = 0.25$ the predicted values of τ_m were computed and are given in table 2 for the other experimental conditions. In general it can be seen that the model is in reasonable agreement with the observed trends. The weak dependence on temperature and molecular weight distribution are consistent with experimental findings. In addition the decrease in relaxation time with increasing entrance velocity gradient $\dot{\epsilon}_m$ is clearly apparent.

The essential feature of our model that predicts the observed centre-line relaxation behaviour reported in this paper is related to our proposal that only molecules with a relaxation time greater than $\tau \geqslant \alpha/\dot{\epsilon}_m$ will contribute to the initial birefringence. Thus while a change in temperature and/or molecular weight distribution will have the effect of changing the relaxation time distribution of the polymer, this will essentially only result in more or fewer molecules satisfying the condition $\tau \geqslant \alpha/\dot{\epsilon}_m$ and consequently only the number of molecules contributing to the birefringence and stress will change with changing temperature and molecular weight distribution. From this argument a decrease in temperature and/or an increase in the molecular weight distribution will have the effect of shifting the relaxation time distribution to higher values of τ. This will have no major effect on τ_m but will increase the number of molecules contributing to the stress and birefringence. This effect is consistent with the observed manner

TABLE 2. THE DEPENDENCE OF RELAXATION TIME ON TEMPERATURE, MOLECULAR WEIGHT AND $\dot{\epsilon}_m$

parameters kept constant	variable parameter				
$\bar{M}_n = 20000$	T/°C	144	150	170	190
$\bar{M}_w = 130000$	τ_i/s	0.015	0.016	0.017	0.016
$\dot{\epsilon}_m = 38\ s^{-1}$	τ_m/s	0.0153	0.0152	0.0147	0.0143
	$\bar{M}_n$	9000	14000	20000	
$T = 190$ °C	$\bar{M}_w$	90000	65000	130000	
$\dot{\epsilon}_m = 38\ s^{-1}$	τ_i/s	0.01	0.009	0.016	
	τ_m/s	0.0118	0.0135	0.0143	
$\bar{M}_n = 20000$	$\dot{\epsilon}_m$	9	19	38	
$\bar{M}_w = 130000$	τ_i/s	0.048	0.039	0.016	
$T = 190$ °C	τ_m/s	0.0478	0.0253	0.0143	

τ_i is the experimentally determined relaxation time based on equation (5).

τ_m is the predicted mean relaxation time numerically computed from equation (9) with parameters $\alpha = 0.25$ and $C_1 = 0.006$ s °C.

reported in this paper in which the initial birefringence Δ_0 varies with both temperature T and molecular weight for a given value of $\dot{\epsilon}_m$.

The way to modify significantly the mean centre-line relaxation time of the polymer would be to alter the entrance velocity gradient $\dot{\epsilon}_m$, as it is this factor alone that dominates the observed τ_m in our experimental situation.

The choice of the variable parameter $\alpha = 0.25$ used in the analysis is somewhat arbitrary, although it would be difficult to get reasonable agreement with the results if values outside the range $0.1 > \alpha > 0.4$ were chosen. The implication from this result is that the condition $\dot{\epsilon}\tau > 0.25$ is necessary for polymer melts and not $\dot{\epsilon}\tau > 1$ as proposed from dilute solution theory.

We equate the residue birefringence Δ_r with the contribution from the network. We envisage that above a limiting value of $\dot{\epsilon}_m = 5\ s^{-1}$ within the entrance region the network will be deformed affinely and will be stretched in the direction of flow by an amount equal to the change in cross-sectional area of the duct, namely 15/1. When the drawn network enters the slit along the centre line, unlike a rubber, the network is unable to relax instantly because the network resides within the matrix of lower molecular weight material. The relaxation of the network apparently takes 10–1000 s and thus is not observable for the residence time of our experiments within the slit. Thus the birefringence Δ_r seen at the slit exit is assumed to be essentially the unrelaxed contribution of the network deformation that has occurred in the entrance region.

4.2. *Entrance region effects*

The basic elements of our model are shown schematically in figure 37 for the whole duct. Within the entrance region we argue that there are two contributions to the molecular orientation and hence the birefringence and stress. Consequently the birefringence at the throat Δ_m is the sum of the birefringence due to the oriented matrix Δ_0 and the stretched network Δ_r:

$$\Delta_m = \Delta_0 + \Delta_r. \tag{10}$$

On this basis and supported by figures 23 and 24, we would expect Δ_0 to depend on $\dot{\epsilon}_m$, and possibly T, and Δ_r to be essentially independent of $\dot{\epsilon}_m$. The observed difference in the way

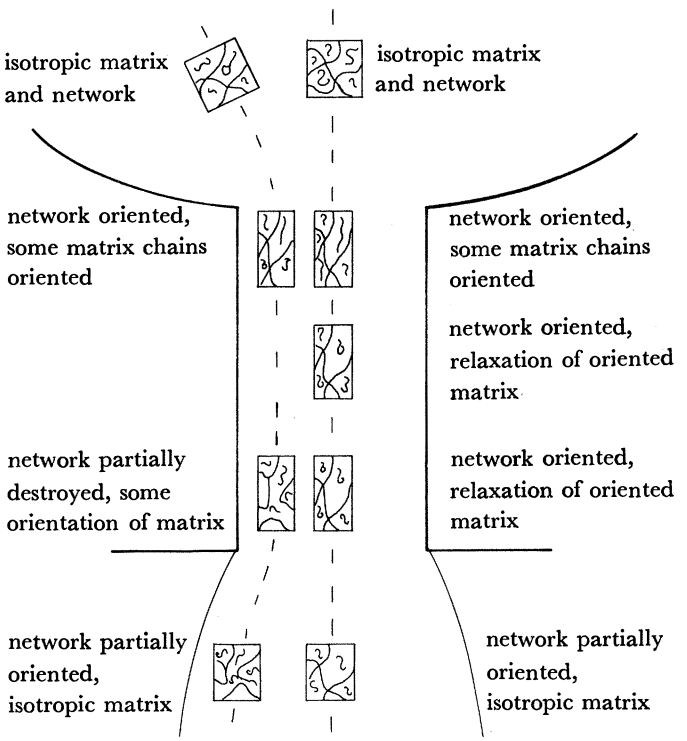

FIGURE 37. Schematic diagram of the manner in which commercial polymer melts flow through duct.

these contributions behave, particularly as a function of $\dot{\epsilon}_m$, is consistent with our belief that the origin of the two contributions is different.

From classical rubber elasticity theory it should be possible to predict the birefringence contribution Δ_r for the network. Treloar (1975) formulates the problem for a Guassian network containing N_n chains per unit volume. The major weakness of the model in relation to the present work is that the chains are assumed to have the same degree of polymerization and unfortunately we do not know of any work that takes molecular weight distribution into account. Treloar derives an expression for the birefringence of a rubber in the form

$$\Delta = \frac{2\pi}{45}\frac{(n_0^2+2)}{n_0}(\alpha_1-\alpha_2)\,N_n\left(\lambda^2-\frac{1}{\lambda}\right), \tag{11}$$

where n_0 is the mean refractive index, $\alpha_1-\alpha_2$ is the difference in principal polarizabilities for each random link of the chain, N_n is the number of chains/unit volume contributing to the network and λ is the extension ratio. Equation (11) can be simplified if the stress optical coefficient is known for the material. This is given by rubber elasticity theory as

$$C = \frac{2\pi}{45}\frac{(n_0^2+2)}{n_0}\frac{(\alpha_1-\alpha_2)}{kT}. \tag{12}$$

Thus

$$\Delta = CkTN_n\lambda^2, \tag{13}$$

when $\lambda \gg 1$, where k is Boltzmann's constant. The coefficient C can be derived experimentally either for cross-linked polyethylenes (see for example Treloar 1975; Gent & Vickroy 1967) or for polyethylene melts (Wales 1976). The values obtained by both methods agree surprisingly

well and for polyethylene at $T = 150\,^{\circ}\mathrm{C}$, $C = 2.4 \times 10^{-9}\ \mathrm{m^2/N}$. If we assume that the network is deformed in the entrance region by a factor of 15 equal to the reduction in cross-sectional area, we derive from equation (13)

$$\Delta/N_n = 3.15 \times 10^{-27}\ \mathrm{m^3}. \tag{14}$$

We further assume that Δ is given by the residue birefringence Δ_r, at $T = 150\,^{\circ}\mathrm{C}$; Δ_r is found typically to be 5×10^{-4} and substitution in equation (14) gives

$$N_n = 1.58 \times 10^{23}\ \mathrm{chains/m^3}.$$

For $\bar{M}_n = 2 \times 10^4$ and $T = 150\,^{\circ}\mathrm{C}$ with the density $\rho = 790\ \mathrm{kg/m^3}$, we would expect the total number of chains per unit volume to be of the order 238×10^{23} which, by comparison with N_n, suggests that only a small but important fraction of the total number of chains within the melt are contributing to the residue birefringence.

The birefringence contribution of the oriented matrix component Δ_0 can be determined similarly. The difference in principal polarizabilities $\gamma_1 - \gamma_2$ of a single chain with degree of polymerization x is given by (Treloar 1975)

$$\gamma_1 - \gamma_2 = (\alpha_1 - \alpha_2)\, x \{1 - 3(r/xa)/\mathscr{L}^{-1}(r/xa)\}, \tag{15}$$

where r is the end-to-end distance of the chain, a is the length of each repeat unit of the chain and $\mathscr{L}^{-1}(r/xa)$ is the inverse Langevin function, which is defined in Treloar (1975).

The principal polarizability difference per unit volume $\partial_1 - \partial_2$ is given by,

$$\partial_1 - \partial_2 = N_{\mathrm{m}}(\gamma_1 - \gamma_2), \tag{16}$$

where N_{m} is the number of chains per unit volume, contributing to the matrix birefringence. Using the Lorentz relation together with equations (12), (15) and (16) gives the birefringence in the form

$$\Delta = 5CkTN_{\mathrm{m}}\, x \{1 - 3r/xa/\mathscr{L}^{-1}(r/xa)\}. \tag{17}$$

It is now necessary to determine the strain of the chain in relation to its undeformed mean square end-to-end distance r_0, which for a random coil is given by $r_0 = xa^{\frac{1}{2}}$. For $\dot{\epsilon}_{\mathrm{m}}\tau > \alpha$, the chains will stretch with the flow. Therefore the strain r/r_0 can be equated to the change in the cross-sectional area of the duct. Thus

$$r/r_0 = 15 \quad \text{and} \quad r/xa = 15\, x^{-\frac{1}{2}}. \tag{18}$$

Assuming $M_n = 2 \times 10^4$ yields the degree of polymerization $x = 714$ and the ratio $r/xa = 0.56$. Using the curve given in figure 9.1 of Treloar (1975), we arrive at the value within the brackets of equation (17) as 0.2. Thus using the values of T and C previously quoted we obtain

$$\Delta/N_{\mathrm{m}} = 1.0 \times 10^{-27}. \tag{19}$$

Equating Δ to the experimental values of Δ_0 we arrive at a value for the number of chains per unit volume as a function of $\dot{\epsilon}_{\mathrm{m}}$:

$\dot{\epsilon}_{\mathrm{m}}/\mathrm{s^{-1}}$	3	10	18	35
$10^{-23}\ N_{\mathrm{m}}/(\mathrm{chains/m^3})$	4.5	8	11	16

From this result we see that the number of chains per unit volume contributing to the matrix birefringence progressively increases with increasing $\dot{\epsilon}_{\mathrm{m}}$, and for all values of $\dot{\epsilon}_{\mathrm{m}}$ quoted is greater than the value of 1.5×10^{23} chains per unit volume estimated for the network contribution. However, even at $\dot{\epsilon}_{\mathrm{m}} = 35\ \mathrm{s^{-1}}$, the fraction of chains contributing to the matrix birefringence is still only about 7% of the total estimated number of chains.

PHILOSOPHICAL TRANSACTIONS OF THE ROYAL SOCIETY A MATHEMATICAL, PHYSICAL & ENGINEERING SCIENCES

4.3. *Exit effects*

Figure 37 gives a schematic picture of how we envisage relaxation to occur when the polymer emerges from the slit. The initial relaxation χ_i is thought to be attributed to the relaxation of the matrix material, and this relaxation takes place within the time scale of our optical observations. The decrease of χ_i with L/D is attributed to the centre-line relaxation effect. Subsequent annealing of the extrudate allows the network contribution to relax and it is this component that is thought to account for the swelling contribution $\chi_\infty - \chi_i$. Our experimental swelling data is given for polypropylene. However, we have established that HDPE swells similarly, although for high molecular weight polyethylene the ultimate swell ratio for a knife edge die can exceed 12.

We consider figure 36 to be important in that it shows the ratio χ_i/χ_∞ increases with increasing L/D. This indicates that χ_∞ decreases more rapidly with L/D than χ_i. We attribute this effect to the fact that the network is being sheared in the regions near the side walls of the slit and is being partially destroyed or modified by the large strains that it will experience. Thus with increasing L/D an increasing amount of network is destroyed, which leads to a decrease in the ultimate swell ratio.

While die swell is of great importance in terms of commercial processing, we are at present not optimistic that it is possible to model mathematically the behaviour of unconstrained swelling for the complex polymer fluids we have examined. We feel that initially more attention should be directed to entrance behaviour and flow within the duct.

5. Conclusion

We have presented evidence that strongly suggests the behaviour of a polymer melt depends not only on velocity gradient history, but also on strain history. We have further shown that the birefringence and stress can be associated with two components within the melt, namely the matrix component, where the contribution to the birefringence and stress depends on the velocity gradient, and the network component, where the birefringence and stress contribution is essentially strain-dependent. Our analysis indicates that less than 1 % of the total number of chains contribute to the network and up to about 7 % at $\dot{\epsilon}_m \approx 35\ s^{-1}$ contribute to the matrix component. These figures suggest that a large fraction of a conventional polymer melt plays an essentially passive role acting as a lubricating matrix for a small but important number of chains that generate orientation and stress. The mathematical complexities associated with taking into account all these factors are formidable and in our view partially explain the difficulties associated with deriving a generalized constitutive equation for commercial polymer melts. In addition it can be seen that even for the relatively simple geometry we have examined, the flow history of fluid elements will be different for different streamlines in the flow. Thus macroscopic effects, such as overall pressure drop and die swell, will necessarily be a complex integration of effects occurring along each streamline.

We have been able to follow the evolution of stress in the entrance region of the duct together with subsequent relaxation behaviour within the slit and at the exit. In particular we have established the boundary conditions at the exit of the slit and for the fluids we examined shown that these conditions were not viscometric. We have also observed the onset of instabilities and established that these grow from small oscillations seen initially at the edges of the throat.

PHILOSOPHICAL TRANSACTIONS OF THE ROYAL SOCIETY A MATHEMATICAL, PHYSICAL & ENGINEERING SCIENCES

Finally, we have presented extensive stress distribution data that we hope we or others may be able to use in future attempts to model the behaviour of melts flowing through ducts.

We wish to thank the S.E.R.C. for financial support of this work. One of us (D.M.) thanks the Churchill Fellowship Trust for supporting him during his stay at Cambridge. Finally M.R.M. wishes to thank Professor A. Keller, F.R.S., and Dr J. Odell for assistance in applying the log normal distribution to the relaxation time problem.

References

Blundell, D. J. & Keller, A. 1968 *J. macromolec. Sci. Phys.*, **132**, 301–336.
Boger, D. V. & Denn, M. M. 1980 *J. Non-Newtonian Fluid Mech.* **6**, 163–185.
Brizitsky, V. I., Vinogradov, G. V., Isayev, A. I. & Podolsky, Y. Y. 1978 *J. appl. Polymer Sci.* **22**, 751–767.
Clegg, P. L. 1958 *Rheology of elastomers* (ed. P. Mason & N. Wookey), pp. 174–189. Oxford: Pergamon Press.
Cross, M. M. 1970 *J. Colloid Interface Sci.* **33**, 30–35.
Gent, A. N. & Vickroy, V. V. 1967 *J. Polymer Sci.* A2 **5**, 47–61.
Han, C. D. 1976 *Rheology in polymer processing*. New York, London: Academic Press.
Han, C. D. & Drexler, L. H. 1973 *J. Appl. Polymer Sci.* **17**, 2329–2354. 2355–2368, 2369–2393.
Han, C. D. & Kim, K. U. 1971 *Polymer Engng Sci.* **2**, 395–400.
Huang, D. C. & White, J. L. 1980 *Polymer Engng Sci.* **20**, 3, 183–189.
Mackley, M. R., Frank, F. C. & Keller, A. 1975 *J. Mater. Sci.* **10**, 1501–1509.
Mackley, M. R. & Keller, A. 1975 *Phil. Trans. R. Soc. Lond.* A, **278**, 29–66.
Middleman, S. 1976 *Fundamentals of polymer Processing*, pp. 463–473. New York: McGraw Hill.
Mori, Y. & Funatsu, K. 1973 *Appl. Polymer Symp.* **20**, 209–220.
Pearson, J. R. A. 1976 *A. Rev. Fluid. Mech.* **8**, 163–181.
Perara, M. G. N. & Strauss, K. 1979 *J. Non-Newtonian Fluid Mech.* **5**, 269–283.
Peterlin, A. 1967 *Polymer* **2**, 257–264.
Treloar, L. R. G. 1975 *The physics of rubber elasticity*. Oxford: Clarendon Press.
Tordella, J. P. 1957 *Trans. Soc. Rheol.* **1**, 203–212.
Tordella, J. P. 1969 *Rheology V5*. (ed. F. R. Eirech), pp. 57–91. London, New York: Academic Press.
Wales, J. L. S. 1976 *The application of flow birefringence to rheological studies of polymer melts*. Delft University Press.
Wesslau, H. 1956 *Makromolek. Chem.* **20**, 124–148.
Ziabicki, A. 1959 *J. appl. Polymer Sci.* **11**, 4, 14–23.

PHILOSOPHICAL TRANSACTIONS OF THE ROYAL SOCIETY A MATHEMATICAL, PHYSICAL & ENGINEERING SCIENCES

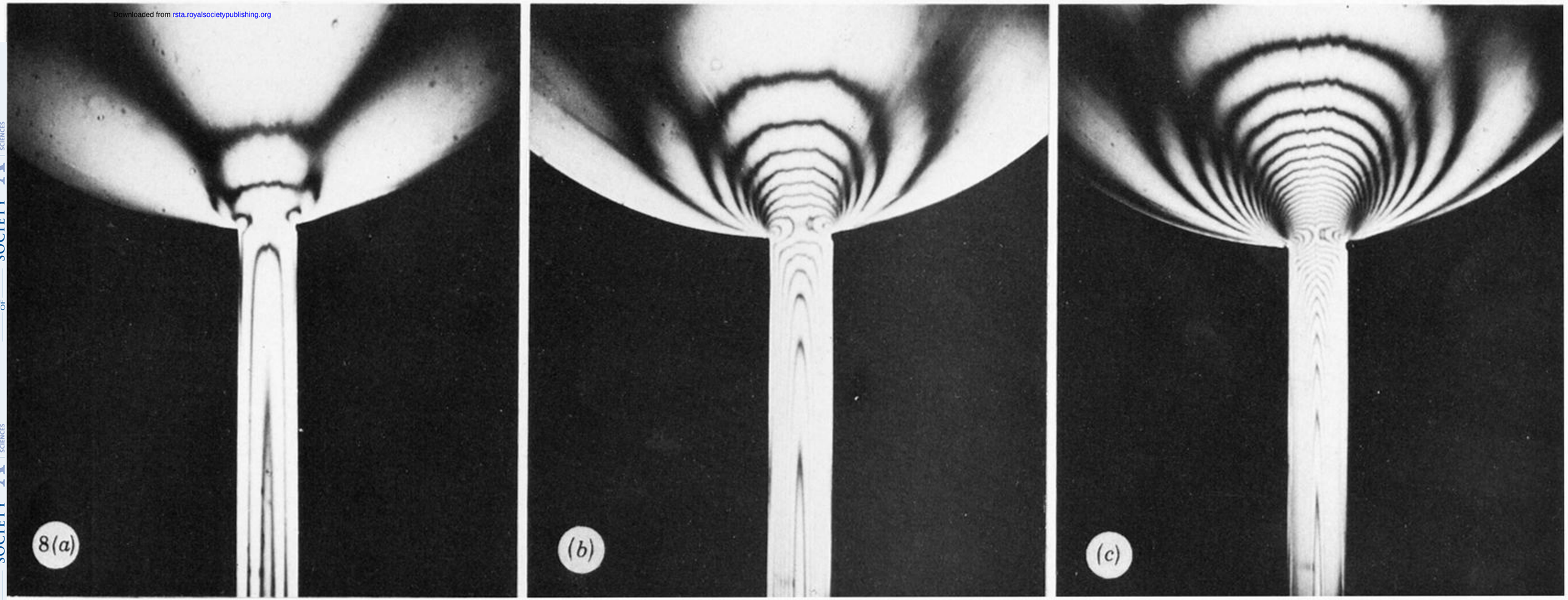

FIGURE 8. Flow birefringence within duct: effect of mean flow (HDPE 006, $T = 170\,^{\circ}\mathrm{C}$). (*a*) $\bar{v} = 10.1\ \mathrm{mm^3/s}$, (*b*) $\bar{v} = 101\ \mathrm{mm^3/s}$, (*c*) $\bar{v} = 395\ \mathrm{mm^3/s}$. Polars are crossed at 45° to centre line.

PHILOSOPHICAL TRANSACTIONS OF THE ROYAL SOCIETY A MATHEMATICAL, PHYSICAL & ENGINEERING SCIENCES

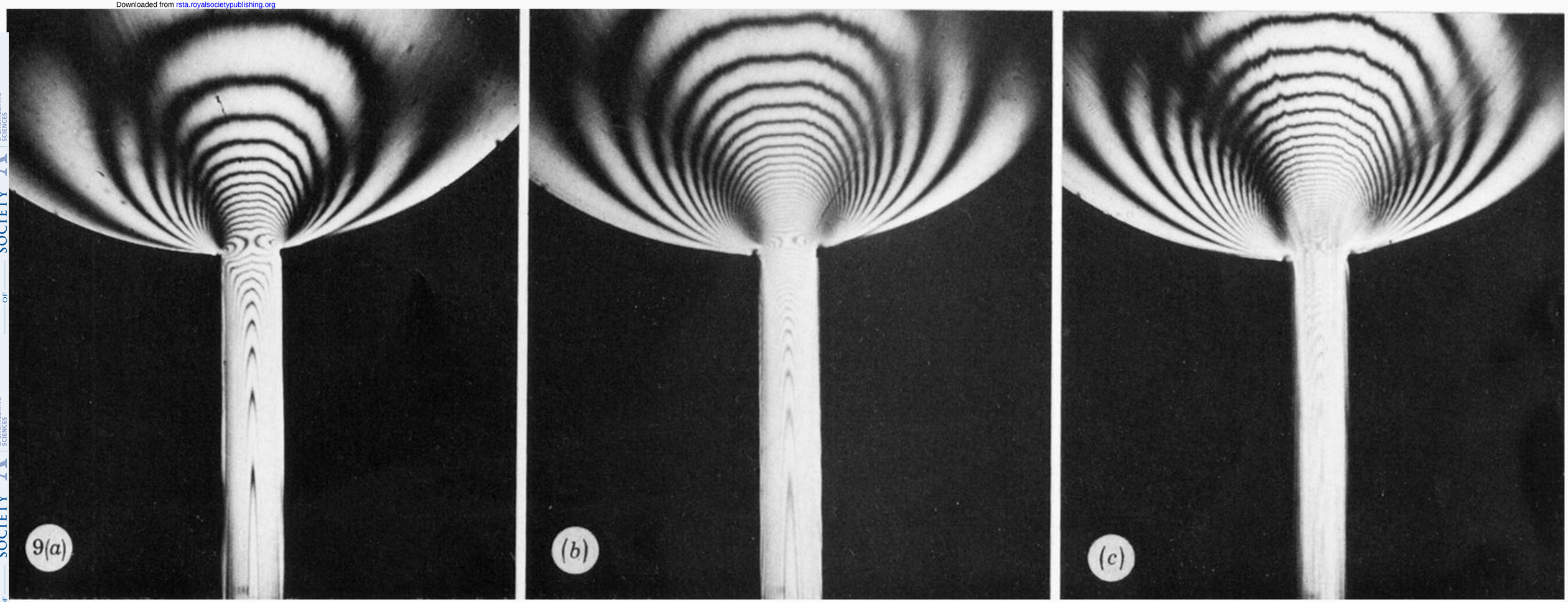

FIGURE 9. Flow birefringence within duct: effect of temperature (HDPE 006, $\bar{v} = 395\ \mathrm{mm^3/s}$). (*a*) $T = 190\ ^\circ\mathrm{C}$, (*b*) $T = 150\ ^\circ\mathrm{C}$, (*c*) $T = 140\ ^\circ\mathrm{C}$. Polars are crossed at 45° to centre line.

PHILOSOPHICAL TRANSACTIONS OF THE ROYAL SOCIETY A MATHEMATICAL, PHYSICAL & ENGINEERING SCIENCES

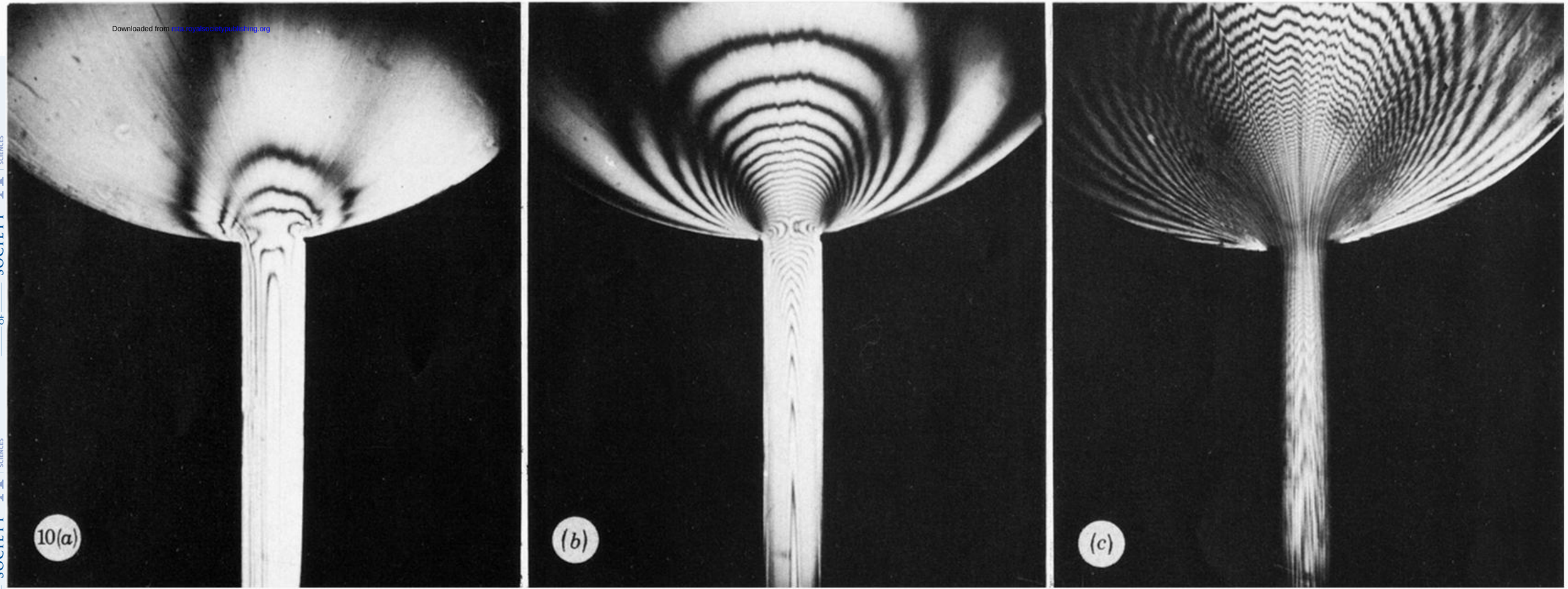

FIGURE 10. Flow birefringence within duct: effect of relative molecular mass ($\bar{v} = 395\,\mathrm{mm^3/s}$, $T = 170\,^{\circ}\mathrm{C}$). (*a*) HDPE 140–60 ($\overline{M}_n = 1.4\times10^4$, $\overline{M}_w = 6.5\times10^4$), (*b*) HDPE 006 ($\overline{M}_n = 2\times10^4$, $\overline{M}_w = 13\times10^4$), (*c*) HDPE 20–54P ($\overline{M}_n = 3.2\times10^4$, $\overline{M}_w = 29\times10^4$). Polars are crossed at 45° to centre line.

PHILOSOPHICAL TRANSACTIONS OF THE ROYAL SOCIETY A MATHEMATICAL, PHYSICAL & ENGINEERING SCIENCES

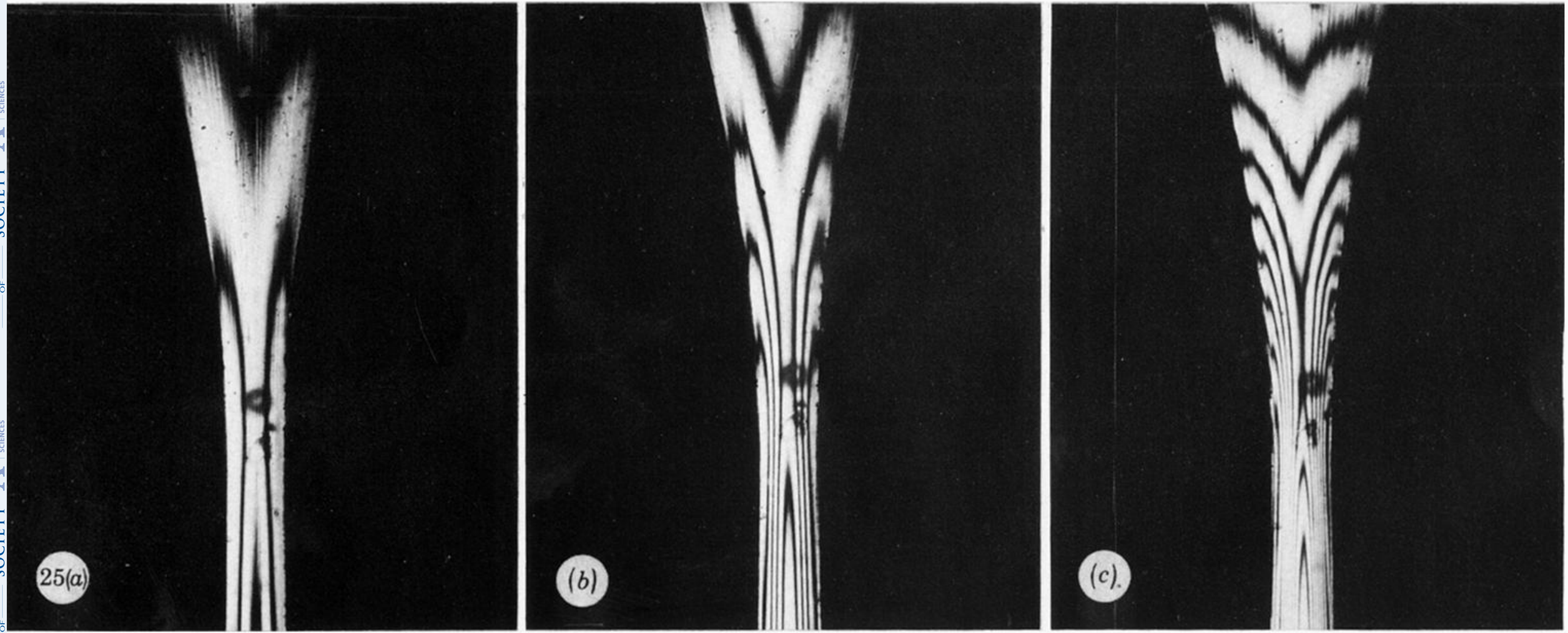

FIGURE 25. Flow birefringence observed for tapered entrance for HDPE 006 at 190 °C: (*a*) $\bar{v} = 42.6$ mm³/s, (*b*) 130 mm³/s, (*c*) 517 mm³/s. Polars are crossed at 45°.

PHILOSOPHICAL TRANSACTIONS OF THE ROYAL SOCIETY A MATHEMATICAL, PHYSICAL & ENGINEERING SCIENCES

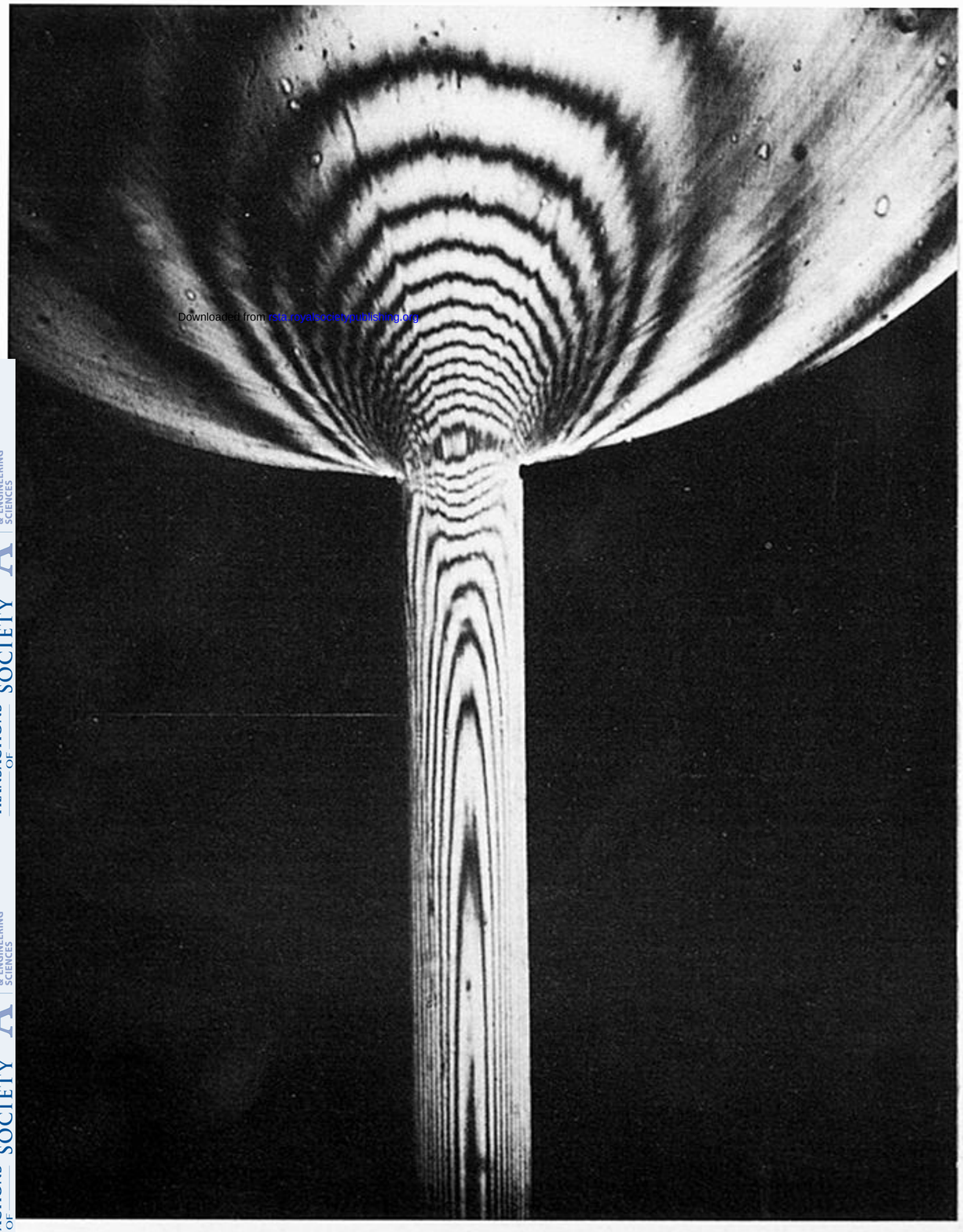

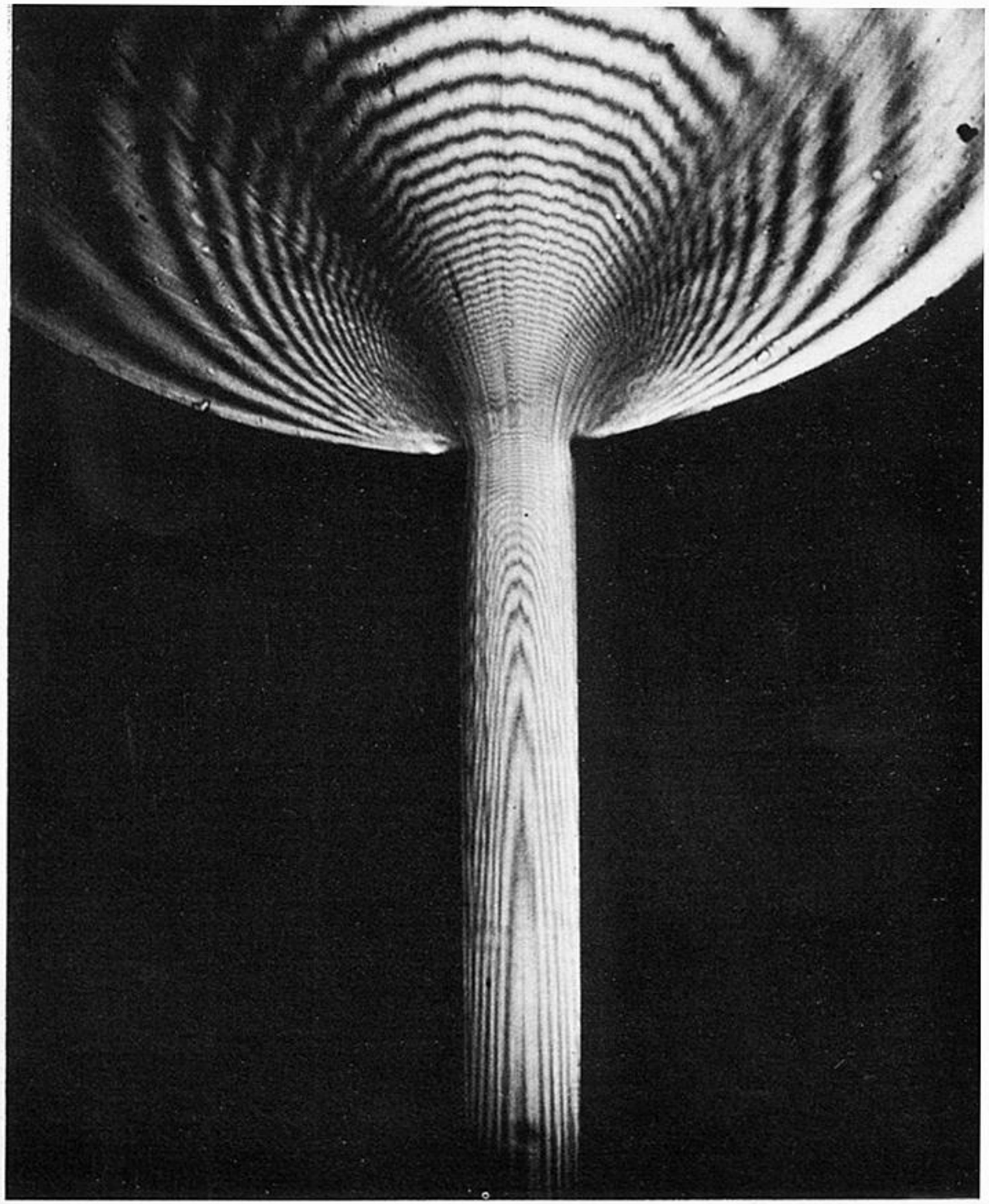

FIGURE 26. Flow birefringence showing 'symmetric oscillation' effect for HDPE 20–54P at 190 °C with $\bar{v} = 258$ mm³/s. Polars are crossed at 45°.

PHILOSOPHICAL TRANSACTIONS OF THE ROYAL SOCIETY A MATHEMATICAL, PHYSICAL & ENGINEERING SCIENCES

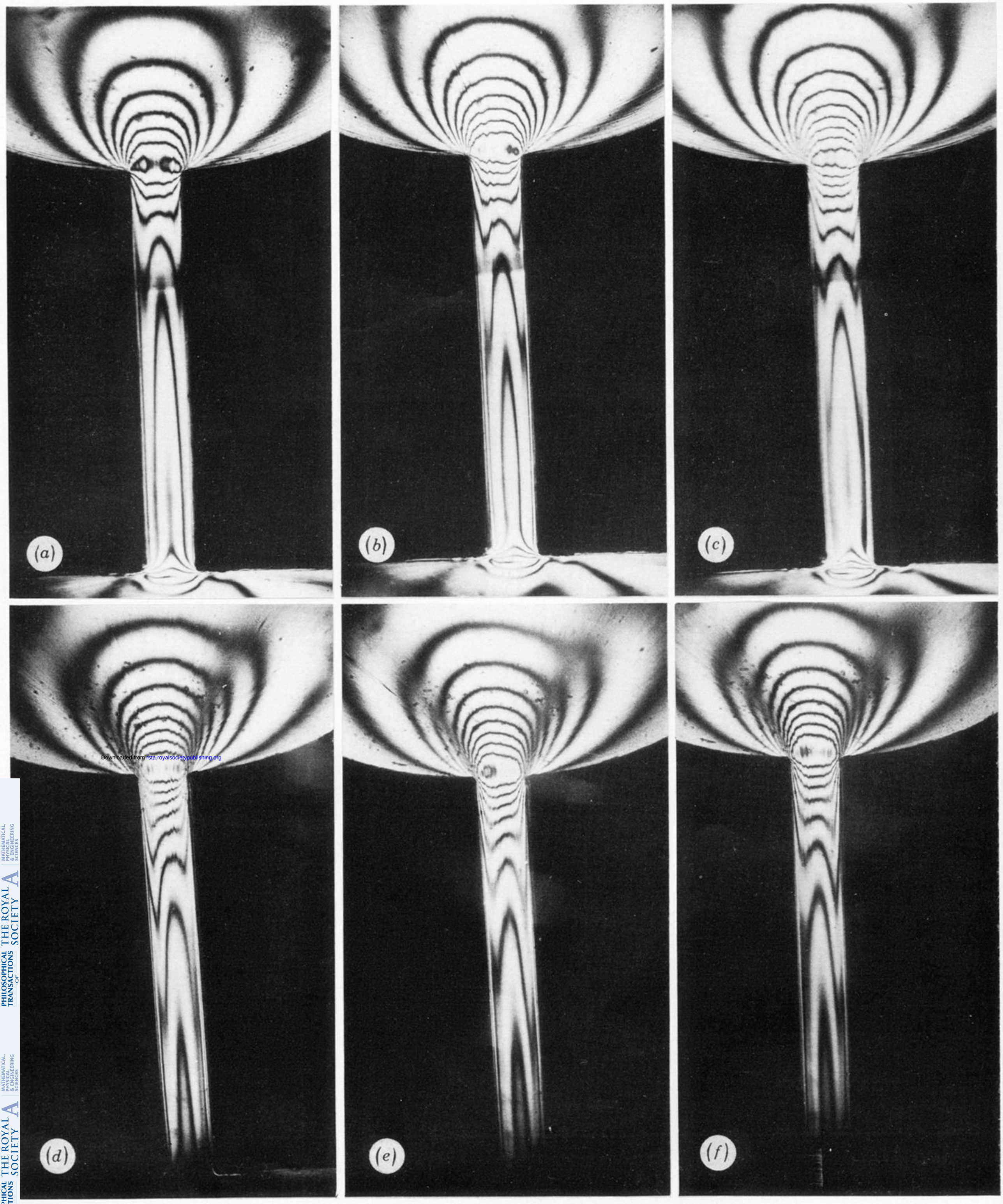

FIGURE 27. Development of W fringes and 'asymmetrical oscillations' for polypropylene copolymer GPE-102 at 193 °C: (*a*) $\bar{v} = 300\ \mathrm{mm^3/s}$, (*b*) $\bar{v} = 400\ \mathrm{mm^3/s}$, (*c*) $\bar{v} = 500\ \mathrm{mm^3/s}$. (*d*)–(*f*) $\bar{v} = 510\ \mathrm{mm^3/s}$, Polars are crossed at 4°5.

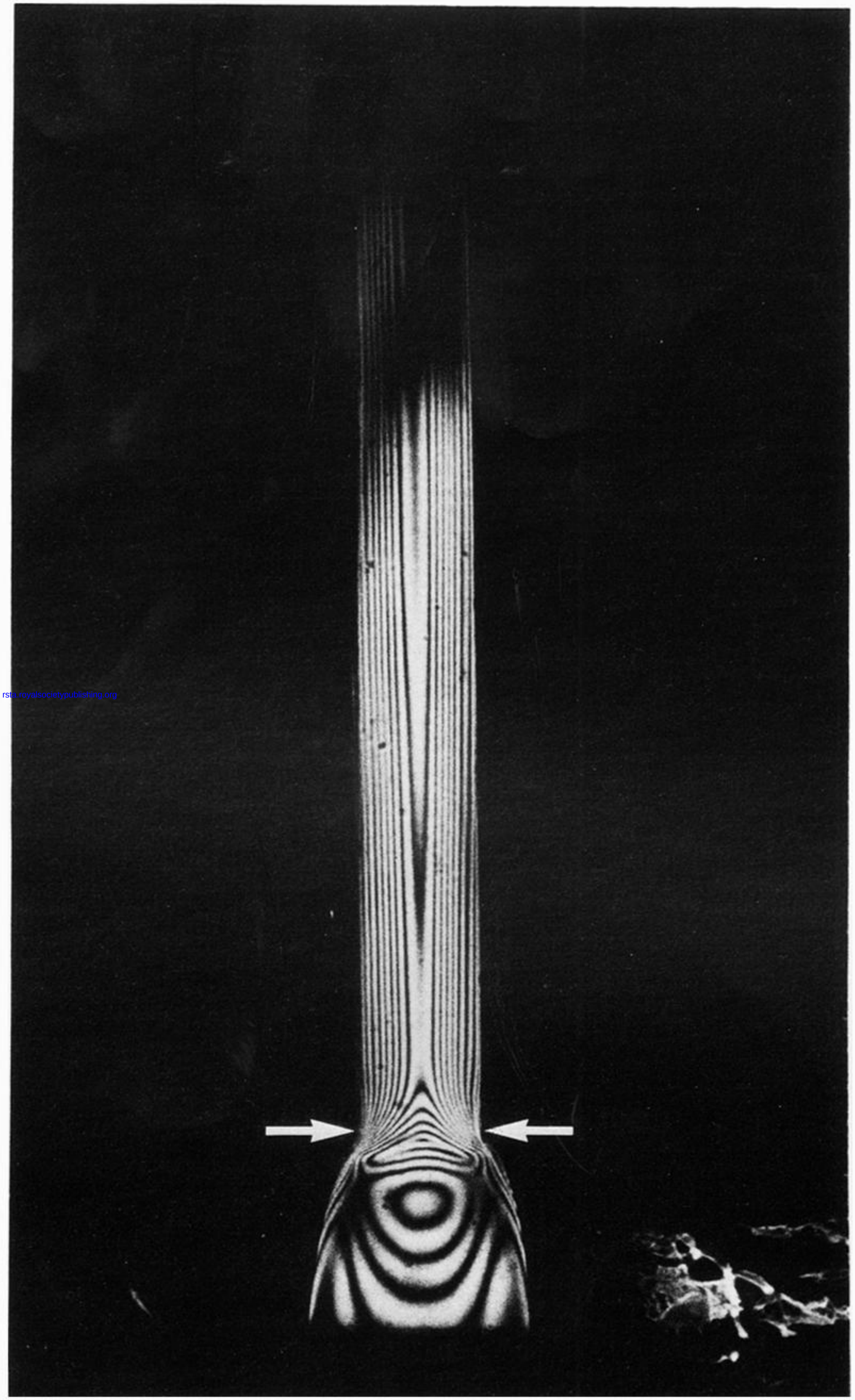

FIGURE 30. Flow birefringence at slit exit for HDPE 02–55 at 210 °C with $L/D = 16$ mm/1 mm, $\bar{v} = 639$ mm^3/s. Polars are crossed at 45°.

PHILOSOPHICAL TRANSACTIONS OF THE ROYAL SOCIETY A MATHEMATICAL, PHYSICAL & ENGINEERING SCIENCES

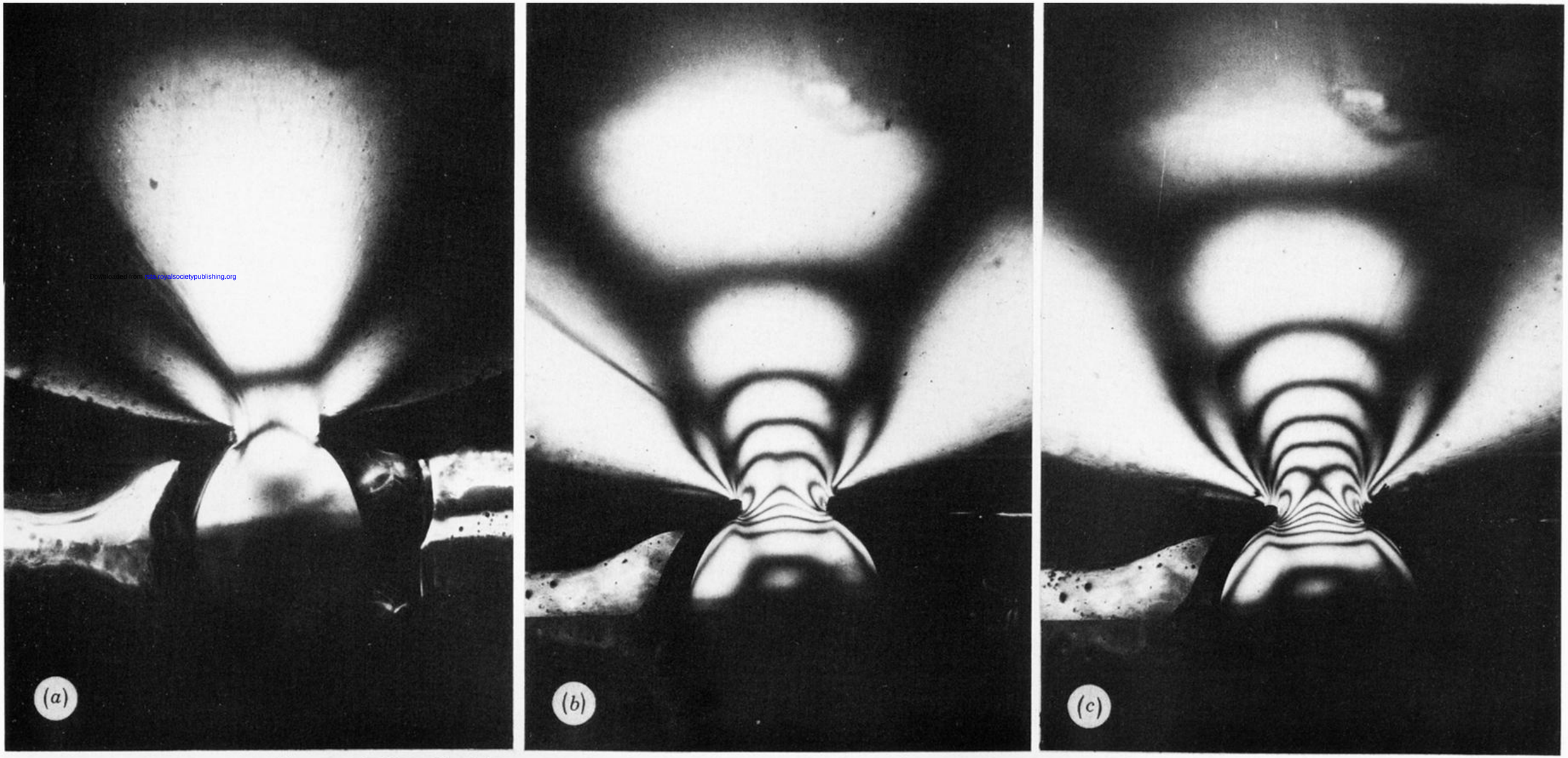

FIGURE 31. Flow birefringence within duct for polypropylene GSE-16 at 230 °C. Polars are crossed at 45°.

(*a*)–(*c*) $L/D = 0.1$ mm/1 mm; (*a*) $\bar{v} = 63$ mm³/s, (*b*) 318 mm³/s, (*c*) 574 mm³/s.
(*d*)–(*f*) $L/D = 2.3$ mm/1 mm; (*d*) $\bar{v} = 63$ mm³/s, (*e*) 318 mm³/s, (*f*) 574 mm³/s.
(*g*)–(*i*) $L/D = 8$ mm/1 mm; (*g*) $\bar{v} = 63$ mm³/s, (*h*) 318 mm³/s, (*i*) 574 mm³/s.
(*j*)–(*l*) $L/D = 16$ mm/1 mm; (*j*) $\bar{v} = 63$ mm³/s, (*k*) 318 mm³/s, (*l*) 574 mm³/s.

PHILOSOPHICAL TRANSACTIONS OF THE ROYAL SOCIETY A MATHEMATICAL, PHYSICAL & ENGINEERING SCIENCES

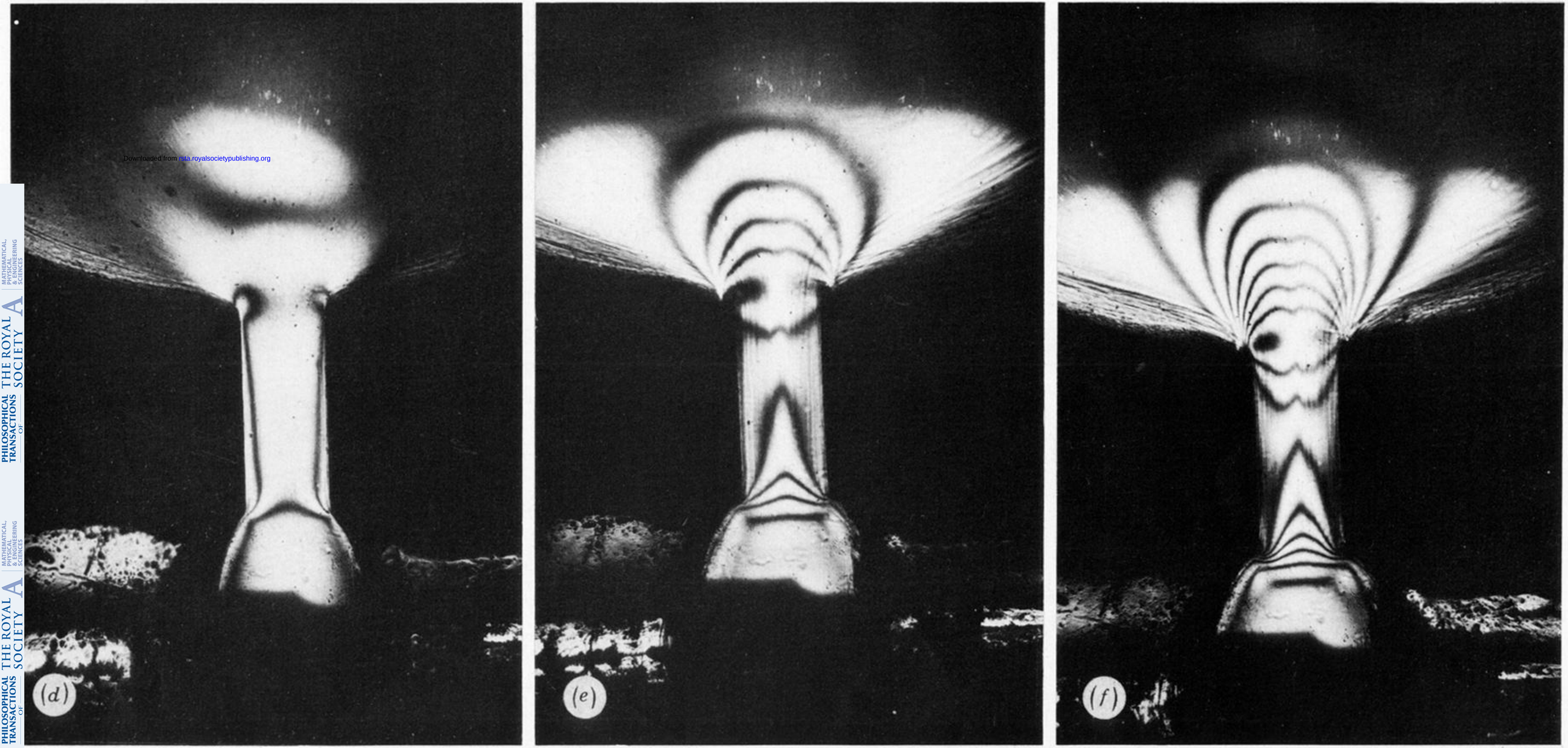

PHILOSOPHICAL TRANSACTIONS OF THE ROYAL SOCIETY A MATHEMATICAL, PHYSICAL & ENGINEERING SCIENCES

FIGURE 31 (*d*)–(*f*). For description see plate 6.

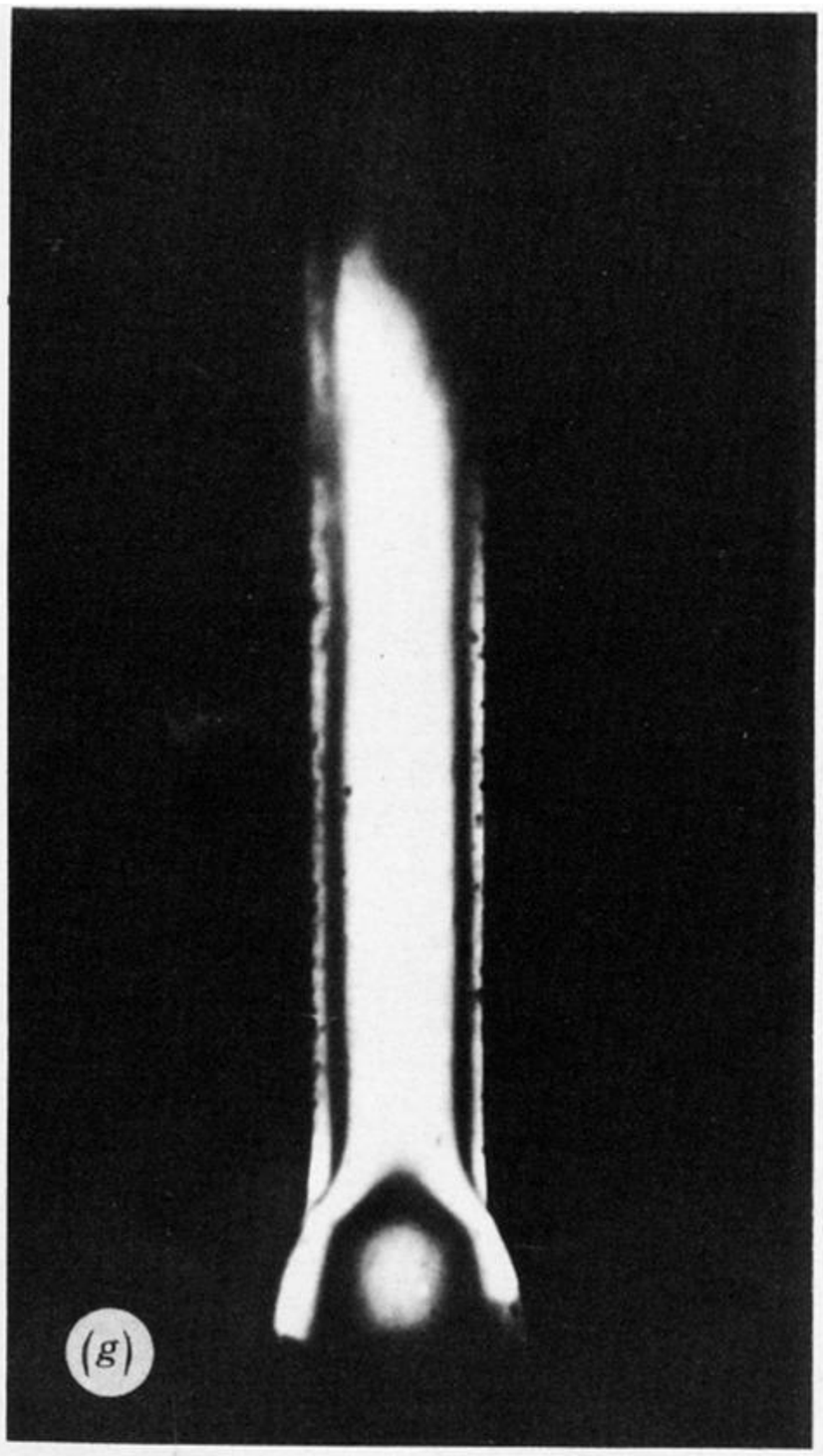

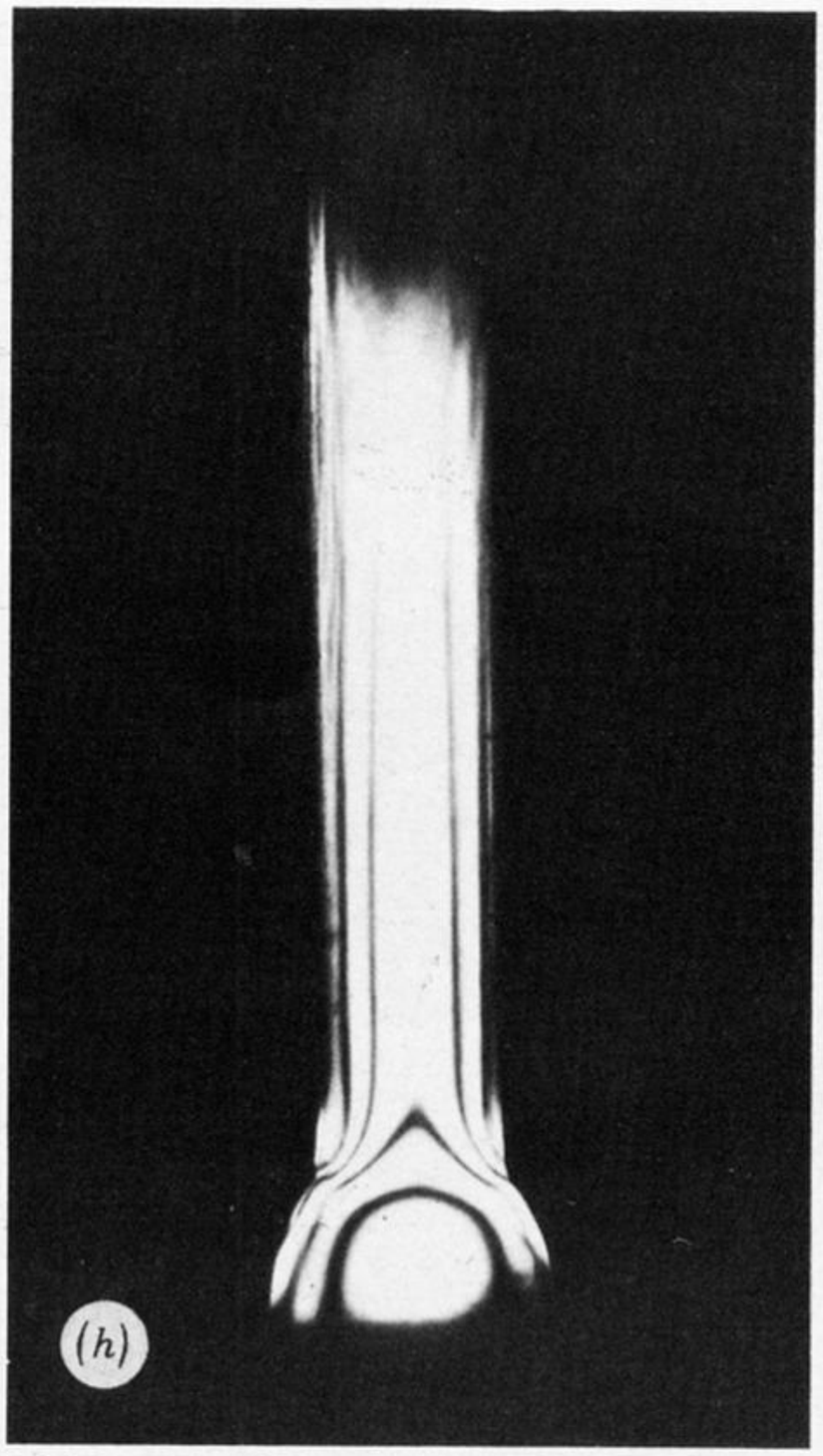

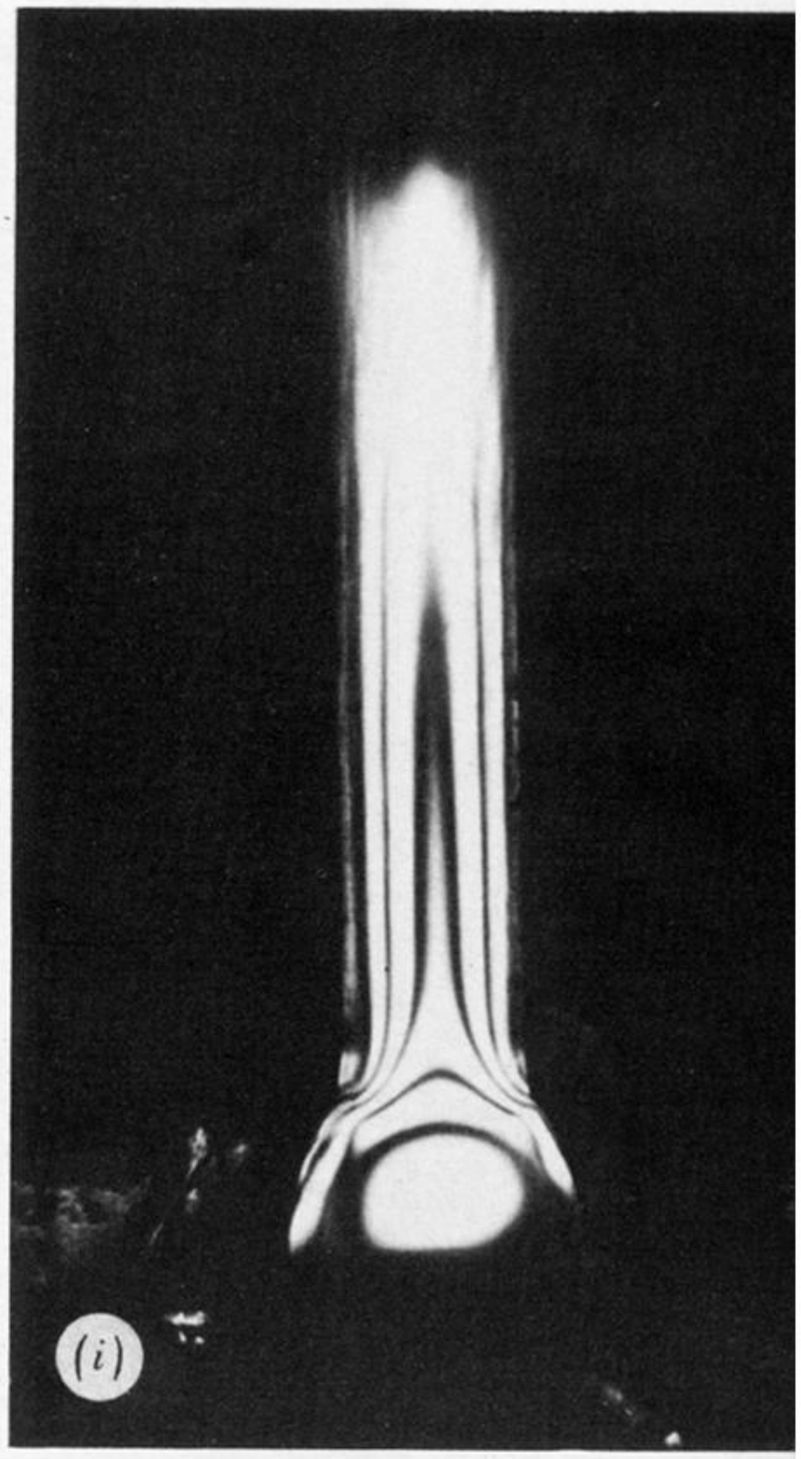

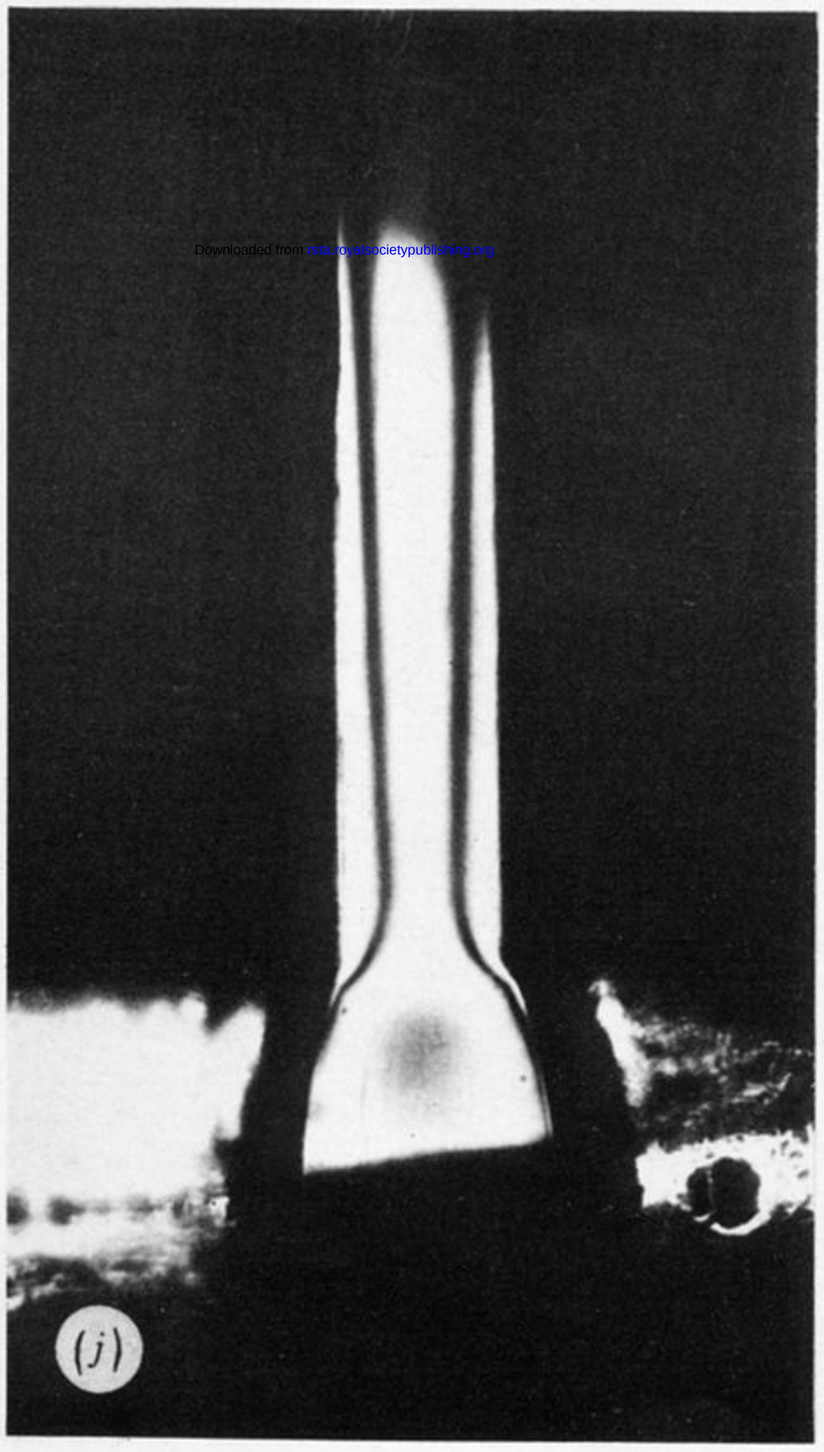

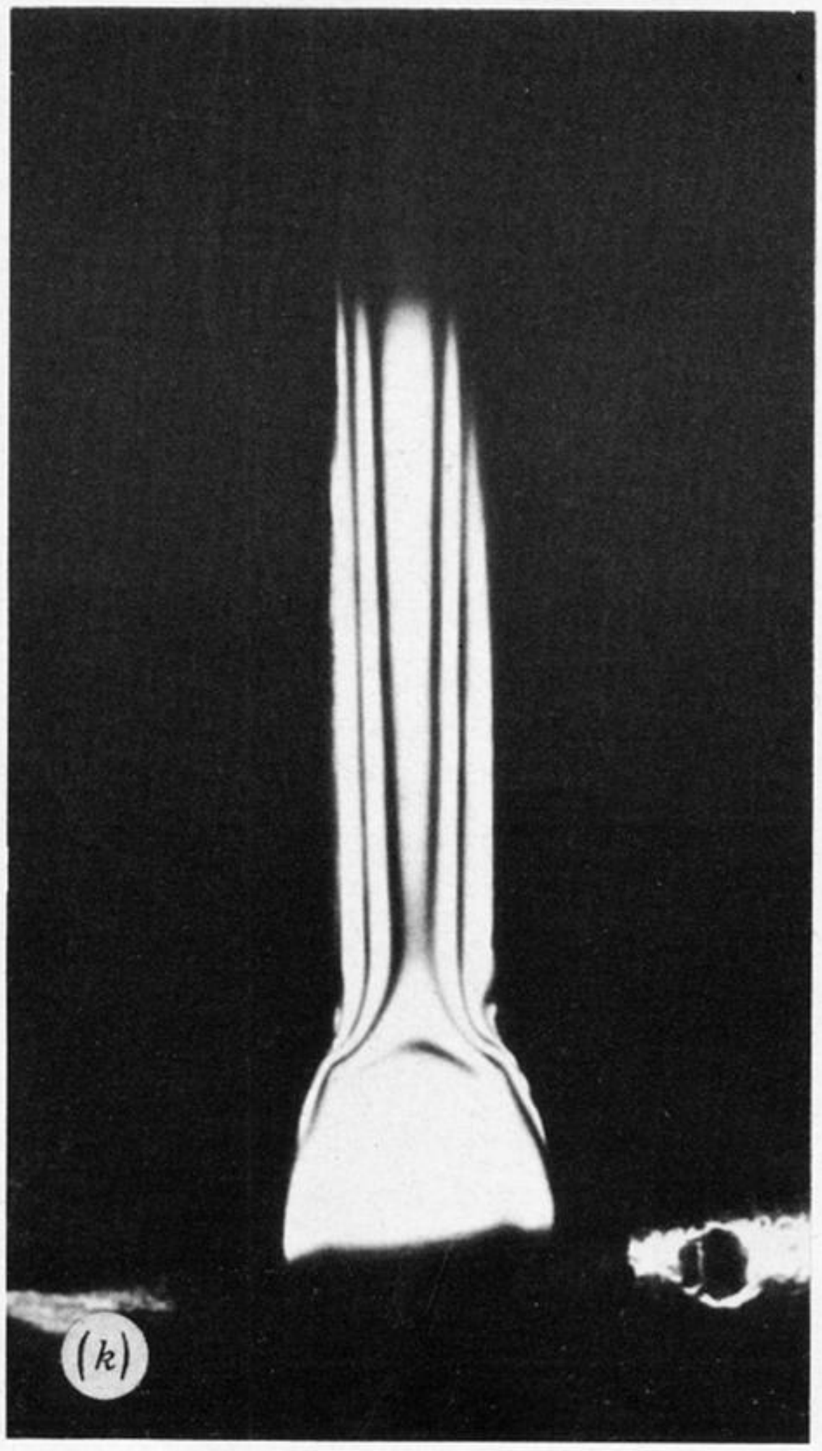

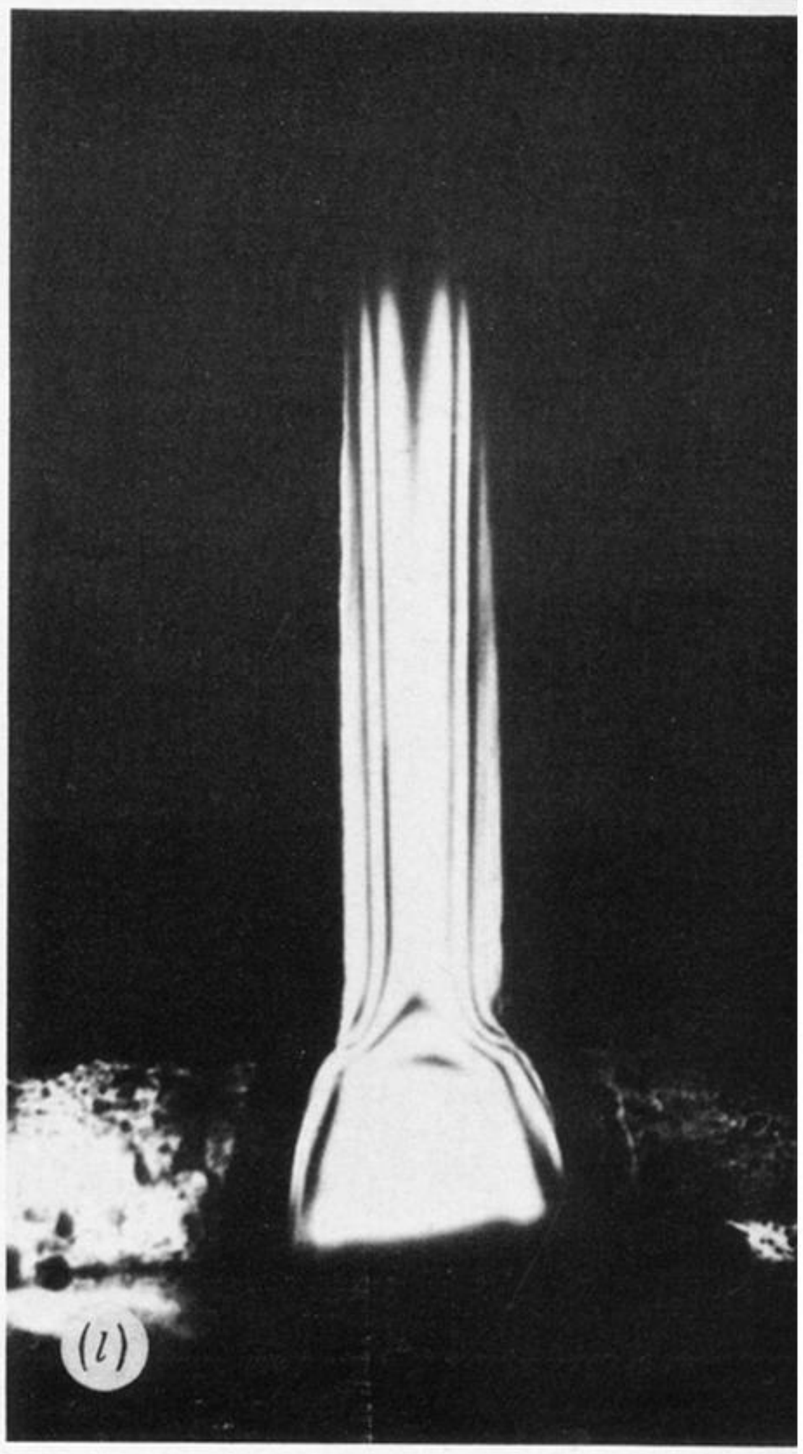

PHILOSOPHICAL TRANSACTIONS OF THE ROYAL SOCIETY A MATHEMATICAL, PHYSICAL & ENGINEERING SCIENCES

FIGURE 31 (*g*)–(*l*). For description see plate 6.